Master thesis

Productivity versus Preservation

Black shale deposition of the Early Toarcian (Jurassic) ocean anoxic event in the Northern German Basin

By

Timothy Florian Baars

Date

July 2017

Supervisors

dr. B. van de Schootbrugge (Utrecht University)

dr. J. Trabucho Alexandre (Utrecht University)

dr. D. Harazim (Louisiana State University)

Abstract

The Early Toarcian Ocean Anoxic Event (OAE) and the corresponding North European black shales reflect a period of enhanced organic matter preservation. Although this event has seen an extensive amount of study the environmental conditions, mechanisms, and processes that resulted in the deposition of the organic-matter-rich sediments are still a matter of discussion and not yet fully understood. In this study, we present a new interdisciplinary approach to the Toarcian black shales from the Northern German Basin. Making use of petrographic, geochemical and palynological analysis, dynamic and previously unnoticed, subtle changes were observed. Two different episodes of black shale depositions are recognized. The first period, in the exaratum subzone, aligns with a global perturbation of the carbon cycle. We argue that this perturbation lead to salinity driven stratification and a stressed upper water column. With a low sea-level at the time of this episode basin restriction formed the perfect catalyst enhancing the anoxic conditions in the basin leading to a preservation driven black shale deposition. Furthermore, the clustered debated sphearicals present in this episode are interpreted to be juvenile *Tasmanites* and indicate environmental stress. During the second episode, in the falciferum subzone, further developing sea-level rise and the inflow of colder, nutrient-rich artic waters led to a shift in the deposition of organic matter. Weakening of the salinity stratification and improvement of life in the upper water column led to enhanced productivity. With dysoxia only prevailing in the deeper parts of the basin the black shale deposition became more productivity driven than the first episode. Within this second period of black shale deposition levels of faecal pellets and the prasinophyte genus *Tasmanites* in the rock record are significantly high.

TABLE OF CONTENTS

1. Introduction

The Early Jurassic was a time of profound change in the atmosphere, geosphere and especially the biosphere. These changes are associated with intense and long-lasting variations in the deposition of organic matter-rich rocks along the margins of the Tethys Ocean (Fig. 1B). The generally organic matter depleted sediments from the Triassic shift towards organic-matter enriched sediments during the Early Jurassic (Van de Schootbrugge et al., 2013). Early Toarcian stage (~183 Ma) sediments of the lower Jurassic show an enrichment in organic matter, reaching almost 20% organic carbon content (Schouten et al., 2000; Röhl et al., 2001; Bucefalo Palliani et al., 2002). These fine-grained sediments, generally termed black shales, represent an episode of enhanced organic carbon deposition and this event is nowadays known as the Toarcian ocean anoxic event (OAE) (Jenkyns, 1985).

A distinct feature of the Toarcian OAE is a pronounced negative carbon isotope excursion (CIE) of 3-4% (Küspert, 1982; Hesselbo et al., 2000; Schouten et al., 2000) followed by a, lesser known, small positive CIE (Suan et al. 2015). The major negative CIE is linked to a period of global warming (Jenkyns, 2003) although the exact cause of this event is still questioned. Some attribute the negative CIE to methane outgassing (Hesselbo et al., 2000; McArthur et al., 2008; Van de Schootbrugge et al, 2013) because of the negative $\delta^{13}C$ signal of CH_4. However, due to an absence of a trigger for the outgassing and the short time period in which this event occurred (<900 ka) this hypothesis is still disputed (Van de Schootbrugge et al., 2005; Svensen et al., 2007; Suan et al., 2008). Another possible explanation for an excursion in the global carbon isotope reservoir is the massive flood basalt volcanism which occurred with the emplacement of the Karoo-Ferrar Large Igneous (Fig. 1A) Province. It is argued that the release of volatiles from this province would have been extensive enough to cause widespread perturbation of the carbon cycle evoking a greenhouse effect, causing a warming of the climate (Svensen et al., 2007; Van de Schootbrugge et al., 2013).

Although the negative Early Toarcian CIE is a globally recorded event, there is no hard evidence that the deposition of Early Toarcian black shales was a truly global and synchronous event. Studied sections from Japan (Gröcke et al., 2011), Argentina (Al-Suwaidi et al., 2010) and Siberia (Suan et al., 2011) suggest that the intensity and timing of black shale deposition was different to sections in Europe. Even within Europe there is a strong diachronous deposition from North to South (van de Schootbrugge et al., 2013). Sites along the northern margin of Gondwana, such as in Marocco (Bodin et al. 2010) and Oman (Immenhauser et al. 1998), do not show any evidence of black shale deposition. Secondly, in most European sections black shales intervals are recorded after the termination of the negative CIE (e.g. Röhl et al., 2005; Hermoso et al., 2013). The negative CIE may have aided the deposition of the Early Toarcian black shales but the deposition of black shales is controlled by a lot of variables and ultimately is dependent on local processes and conditions (e.g. Schieber, 1990; Trabucho-Alexandre et al., 2012). For

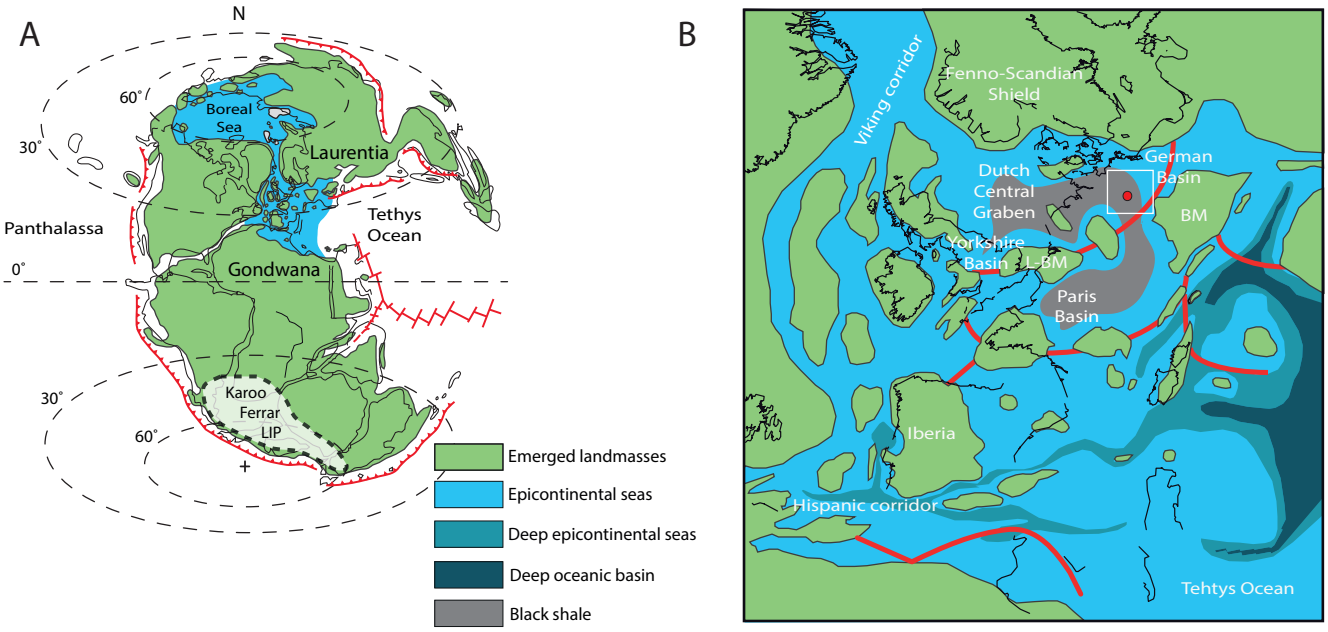

FIG. 1 A) A paleogeographic reconstruction of the world during Toarcian times. B) An overview of the European Epicontinental Seaway with the Toarcian black shale deposition prominent in the basins of northern Europe. The white box and red circle mark the study site and core location (Both figures after Dera et al., 2010)

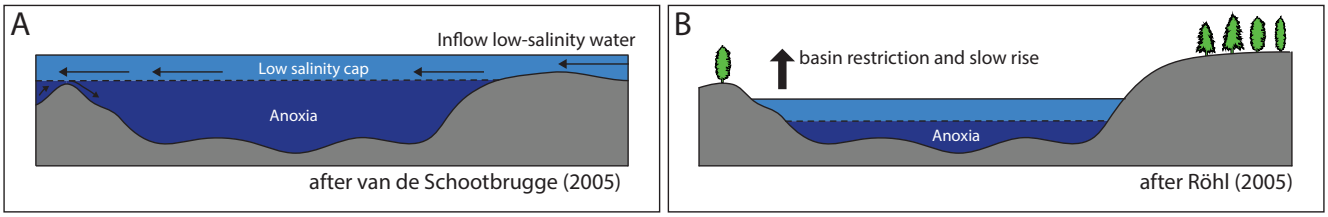

FIG. 2 Two proposed causes for the Toarcian OAE A) Salinity driven density stratification of the water column creating deep water anoxia. B) Deep water anoxia due to basin restriction and the consequent abscence of water circulation.

these reasons, instead of invoking a global mechanism for the Toarcian OAE, most of the current models for the black shale deposition favour a strong regional oceanographic control. The concept of a regional OEA for parts of Europe seems more justifiable (McArthur et al., 2008; Van de Schootbrugge et al., 2013).

1.1 Problem statement

The European Early Toarcian black shales are intensively studied with a vast array of tools and techniques. Based on observations on the sedimentology (Röhl et al., 2001; Wignall and Bond, 2008), changes in phytoplankton populations (Mattioli et al., 2008), organic geochemistry (Schouten et al., 2000) and stable isotope records (Hesselbo et al. 2000; Newton et al., 2011) the enhanced organic matter preservation is commonly interpreted as the consequence of anoxic waters. Despite all this research the exact environmental conditions that lead to the development of the enhanced preservation are still being debated. At the moment two different models are favoured (Fig. 2).

The first model suggests salinity is one of the main controlling factors on the deposition of the black shales. (Fig. 2B) (McArthur et al., 2008; Dera et al., 2009; Van de Schootbrugge et al., 2013). Van de Schootbrugge et al. (2005) advocates that a salinity gradient may have existed with increasing salinity from north to south. The ocean circulation during this period would have transported low-salinity, fresher water from Boreal Basin southward to the European waters (Bjerrum et al., 2011). These low-salinity waters would have led to strong density stratification and to photic zone anoxia (PZA) (Fig. 2a). However, other models suggest that this southward flowing ocean current appeared later in time (Korte et al., 2015). Another source of enhanced low-salinity water input could be related to increased weathering rates and riverine runoff due to the warming conditions. This runoff, if large enough, may also have promoted the development of haline stratification (McArthur et al., 2008; Dera et al., 2009).

A second theory focusses on the sea-level fluctuations throughout this period and the development of anoxic conditions due to basinal restriction. During the Early Toarcian, a second order transgression phase in sea-level has been observed (Haq et al., 1988; Hallam et al., 2001). A model suggested by Röhl et al. (2005) (Fig. 2b) infers that these sea-level variations are the main forcing factor for the black shale deposition and anoxia. A sea-level fall would have caused enclosure of basins and a break in the palaeoceanographic circulation. A successive slow sea-level rise during the Early Toarcian would have induced long-term stagnant conditions with anoxic bottom waters due to basinal restriction and an absent palaeoceanographic circulation.

The interpretation of Röhl et al. (2005) argues that black shales in the European basins would not have been deposited during high sea-levels but on the contrary, during relative low sea-levels. With this concept, the models are mutually exclusive of each other. Having the two environmental scenarios at the same time is impossible because the low sea-level out rules the input of low-salinity boreal water into the basin.

1.2 Research hypothesis

In this study, we attempt to examine which of the two competing models for the Early Toarcian CIE is the most plausible. With the models being mutually exclusive, but also both with enough supporting evidence, timing is a crucial aspect of this question. The sea-level could be high at one point in time and low, somewhat later. Therefore, resolving temporal changes during the Early Toarcian OAE is one of the key aspects of this question and should be better developed. Up to know most of the current literature on the subject has not considered this temporal issue due to a whole rock approach.

A recent paradigm shift in black shale sedimentology indicates that OAE's and black shales are more dynamic than previously assumed. The general, coarse, whole-rock approach is not fully able to reveal subtle changes in the record. Whole rock analyses of any kind homogenize beds of dissimilar origin. The black shales may, on first sight, occur to be planar laminated beds of fine-grained sediment, but detailed analysis via thin sections can provide valuable information about the depositional settings (e.g. Schieber et al., 1990; MacQuaker et al., 2003; Trabucho-Alexandre et al., 2012; Plint et al., 2013). This microstratigraphic analysis enables the detection of subtle changes and does not homogenize beds of dissimilar origin.

The evidence of strong changes in the organic matter (Suan et al., 2015) suggest that the Early Toarcian black shales also could be more dynamic then previously assumed. The strong changes imply that that the interval and cannot be characterized by a period of uniform ocean anoxia and organic matter deposition. To fully investigate the heterogeneity of the black shales, looking at a higher resolution is still insufficient. Microstratigraphy has to date never been investigated in conjunction with palynology. Combing the microstratigraphy with the actual composition of the organic matter allows not only the observation of changes in depositional style but also the observation of changes in the water column. Linking this with additional geochemical data creates a new, integrated approach which is much more diagnostic than conventional black shale analysis and will provide enough analytical power to solve the stated problem. Because this is the first time such an approach is used to evaluate black shales this study also suits as a case study for the new method.

To take such an integrated approach we examined the Posidonia shale formation in the Northern German Basin (NGB) on textural, compositional and organic fabric content. The aims of this study are (I) to carry out a high resolution petrographic study of the black shales of the Posidonia shale formation in the NGB, (II) to compare the organic palynomorphs and geochemical data of these black shales to their physical rock record, and (III) to create a renewed paleo-environmental deposition model that shows the complex deposition history across the Toarcian OAE thereby testing the existing, contradicting, models.

2. Geological setting

During the Early Jurassic, Europe and the North Atlantic regions were characterized by relative high sea-levels and were mainly covered by sea. This water mass, the European Epicontinental Seaway (EES), was an east-west trending shallow shelf sea subdivided into several basins and covering most of North-West Europe. (Fig. 1B) (Ziegler, 1982). The EES formed a connection with the low-latitude Tethys Ocean in the south whereas in the north the Viking Corridor connected the EES to the Boreal Arctic Sea (Bjerrum et al., 2001). The western margin of the EES is argued to be connected to the Pacific Ocean via the Hispanic Corridor (Aberhan, 2001). During Early Toarcian times the EES was located between 20 and 50° N paleolatitude (Ziegler, 1982; Röhl et al., 2005) and the climate at this time was most likely characterized by seasonal influences with strong monsoonal rainfall during periods of summer and high evaporation rates during periods of winter (Röhl et al., 2005 and references herein).

The study site is positioned in the north of the German Basin near the town of Schandelah (52°18'23"N, 10°42'66"W; Fig. 1B) and throughout the Early Toarcian the German Basin paleolatitude was located near the modern sub-tropics (paleolatitude 43.0° N; van Hinsbergen et al., 2015). The c. 15m of black shale deposition at this side of the German Basin corresponds to the Posidonia shale formation. Combined with the

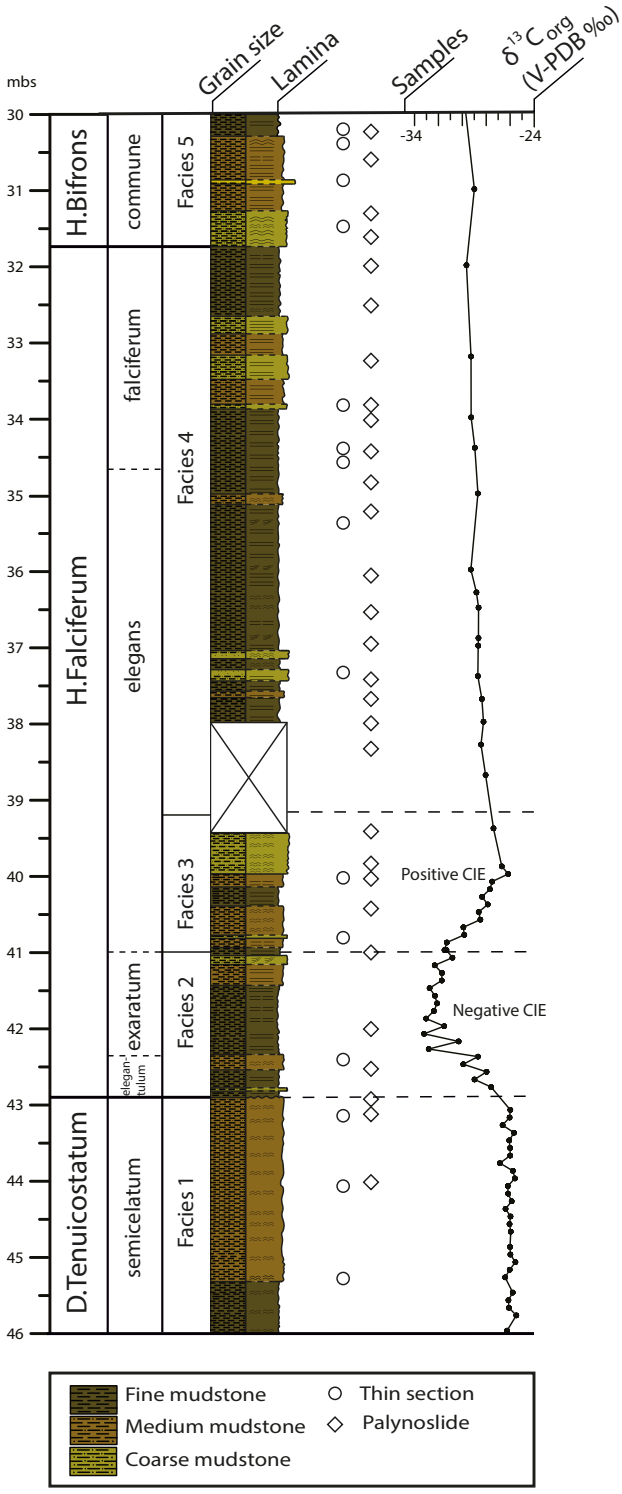

FIG. 3 A statigraphic log of entire examinend interval. From left to right the zones and subzones, determined facies, grain-size, lamina, sample location and $\delta^{13}C_{org}$ values. A clear negative CIE followed by a smaller positive CIE can be observed in the exaratum and early elegans subzone.

Southern German Basin, Dutch Central Graben (both Posidonia Shale Formation), Paris Basin (Schistes Cartons) and the Cleveland Basin (Rock/Mulgrave Shale Member) it forms the prominent deposition site for Toarcian black shales.

Cyclostratigraphic analysis by Suan et al. (2008) assigned a duration of 1.9 myr for the Early Toarcian, however other studies argue a duration close to that of 2.3 myr (Ogg., 2004). The period can be dived into three zones (*D. tenuicostatum*, *H. falciferum*, and *H. Bifrons;* Fig. 3) based on ammonite classification. The lowest *Dactylioceras tenuicostatum* (*D.* polymorphum in southern Europe) zone represents the onset of the Toarcian OAE. In basins across Northern Europe the *D. tenuicostatum* zone is probably only represented by its very topmost part due to a long lasting erosional phase at the start of a second order transgression (Haq et al., 1988; Hallam et al., 2001). The successive *Harpoceras falciferum* (*H. serpentinum* zone in southern Europe) is characterized by the organic rich black shales and the large CIE (Jenkyns, 1985). The CIE is argued to occur during a period of ~900 ka (Suan et al., 2008) in the exaratum sub-zone of the *H. falciferum*. The succeeding *Halosphaera bifrons* zone is the first zone of the Middle Toarcian age. In several places in northern Europe the transition from the *H. falciferum* to the *H. bifrons* zone is characterized by the end of the second order sea-level rise and the deposition of a condensed sections (e.g.; Haq et al., 1988; Hallam, 2001; Röhl et al., 2005).

3. Methods

For this study, core material was used from the Schandelah core in the Lower Saxony Basin, Germany (52°18´23"N, 10°42'66"W). In 2008 a consortium established at the Goethe University Frankfurt obtained a 338-meter-long core from the Northern German Basin that spans from the Rhaetian to the Toarcian and wherein the Toarcian OAE is well captured (Van de Schootbrugge in press). From this core, a sixteen-meter interval covering the Early Toarcian zones was logged, based on core photographs.

For the petrographic analysis and facies descriptions fifteen samples at a c. 1m frequency were studied. In order to visualise the bed and lamina structures, unusually thin (20-25 μm) standard-sized (24x46 mm) polished thin sections were prepared from fresh drill core. The thin-sections were prepared by a commercial lab, Wagner Petrographic (122 N 1800 W #7, Lindon, UT 84042, USA). Using an Epson Perfection V600 Photo scanner and Adobe Photoshop™ all thin section were scanned. Detailed scans of the thin sections enable the observation of 10^{-2} to 10^{-3} m-scale micro textures in these fine-grained sediments. This resolution provides additional information between the standard hand specimen observations from the drilling core and the small scale thin section observations (e.g. Macquaker et al., 2003; Plint, 2014).

Based on these scans detailed logs were made of the different facies. At a higher resolution, the fabrics present within the individual beds and lamina sets were determined making use of a Leica DMRX petrographic microscope attached to a Leica MC170 HD digital camera with 5-megapixel resolution. Approximately 10 photographs were made from each thin section at different magnifications. Some of the photographs were enhanced using Adobe Photoshop™. By making use of three different levels of scale a good representation of the sedimentological dynamics can be constructed. The rock description is based on the nomenclature of Macquaker et al. (2003) and Lazar et al. (2015).

From the same core thirty samples, at a c. 0.5m frequency, were studied for palynological analysis and the determination of different palynomorphs (organic-walled microfossils including spores, pollen and algae). The samples were processed for palynology using standard techniques. Of each sample c. 5g was freeze-dried, crushed and per sample hydrochloric acid (HCL, ~10%) and hydrofluoric acid (HF, ~38%) was added to dissolve carbonates and silicates respectively. Subsequently the samples were sieved over a 10 μm sieve, treated in an ultrasonic bath and placed on a slide with a glycerine gel. For the optical analysis, a Leica DM 2500 LED microscope attached to a Leica MC170 HD digital camera with 5-megapixel resolution was used.

The trace element data used for the study was already generated in a previous research by Ratz (2011). With a 0.5m sample frequency, a fraction of each sample (1g) of the core was freeze-dried, crushed and powdered to homogenize it. From this c. 120 mg was dissolved in subsequently 5ml hydrochloric acid (HCL), 2ml nitric acid (HNO_3) and 1 ml hydrofluoric acid (HF). After dissolution, the samples were heated and acids were removed by evaporation. Following this, to dilute the sample 1 ml nitric acid was added again. The solutions were analyzed for major (Al, Fe, and Mn) and trace (Ni, Cu and Cr) elements concentrations using an inductively coupled plasma-optical emission spectrometer (ICP-OEP, Perkin–Elmer, OPTIMA 3000).

4. Results

The early Toarcian fine-grained siliciclastic rocks are composed of carbonates, siliciclastics, pyrite and organic matter. In general, the sediments are fine-grained ranging from coarse to fine mudstones. Pyrite occurs in high amounts throughout the whole studied section. The sedimentological descriptions and palynological determination reveal five facies associations that are detailed in Table 1, in photographs (Fig. 4 to 8) and in detailed logs (Appendix 1). The distribution of the facies is indicated in the overview (Fig. 9).

4.1 Facies 1 – Bioturbated silt- and clay-rich mudstones

Upon visual macroscopic observation, the sediments in the lower *D. Tenuicostatum* zone appear to be relatively homogenous with an occasional occurrence of cm-thick beds of coarse-silt to fine-sand (Fig. 4A). These coarser beds show evidence of downlap patterns and have erosive bases with basal scour marks (Fig. 4A). Thin section analysis reveals that in the homogenous sediments mm-thick beds are present. These sediments consist mainly of alternating beds of silt-dominant, silt-rich and clay-rich mudstones. The beds are organized in an upward grading succession with planar or wavy laminae. The lowest, silt-dominant, beds have erosive bases (Fig. 4 C&D). The pyrite content within the facies is relatively high and whole beds of pyrite deposition can be distinguished (Fig. 4 B&E). The pyrite has an euhedral from (Fig. 4E) and is predominantly concentrated at the bottom of the graded beds (Fig. 4B). Pyrite is also present as the infilling of burrows (Fig. 4C) The facies is overall heavily bioturbated and the majority of the burrows are pyrite and fine-silt filled. The burrow diameter ranges from several cm- to mm with most of the burrowed structures showing an elongated elliptical shape. Fossil traces of the *Chondrites* spp. can be recognized. In the facies almost no phosphatic debris is present and the visible organic matter content is relatively low. The organic matter content is pollen dominated (predominately bisaccate pollen, e.g. *Classopollis* spp.) but most of the palynomorphs are degraded (Fig. 4F). Other palynomorphs present are spores (e.g. *Chasmatoporites* spp., *Stereisporites* spp.), dinoflagellates (e.g. *Nannoceratopsis* spp.) and acritarchs (e.g. *Micrhystridium* spp.). Furthermore, opaque and translucent wood fragments are abundant. Trace element data for the first facies show that the redox sensitive elements are relatively low. On the contrary, the detrital elements of Al and Ni are the highest recorded of the whole interval.

4.2 Facies 2 – Bituminous clay-rich mudstones with shell pavements

The second facies described aligns with the negative CIE. Macroscopic observation of the sediments show an interlaminated several cm-thick, clay-rich mudstones interlaminating with cm-thick beds composed of shell pavements and bivalve layers (Fig. 5 A&B). The laminae within the clay-rich beds are of a wavy or lenticular discontinuous type and occasionally silt enriched mm-thick interlaminating beds are recognized. In thin section the bivalve layers are recognized as thick layers (100 µm; Fig. 5D) of wavy strings biogenic carbonate with occasional organized calcite rhomb's and could represent the genus *Bositra buchi* (Röhl et al., 2005). Throughout the whole facies the pyrite content is substantially high but unlike the preceding facies 1 the dominant form of pyrite is framboidal. Secondly, the pyrite diameter decreases to <10 µm and is less clustered then in facies 1. Phosphatic (fish) bone debris is present throughout the whole facies in small amounts. The clay-rich beds have a high content of visible organic matter and mm-thick beds with increased organic matter are recognized. The organic matter content is dominated by relatively large aggregates of amorphous organic-derived debris forming flocks (Fig. 5F) which is defined as by marine snow (Alldredge & Silver, 1988). The marine snow can be observed in the thin sections as well (Fig. 5C). In thin section the shape is draped, compressed and has a distinct orange colour. Besides marine snow, ellipsoidal to spheroidal, extremely thin-walled and folded palynomorphs named 'sphaericals' (Prauss et al., 1991) are present. These simple and apparently featureless palynomorphs belong to the green algae prasinophytes group (reasoning follows in later paragraphs). Within this facies they occur in clustered groups ranging from 10-100 individuals, have an median size of +- 20 µm and can be partially engulfed by marine snow or floating throughout the matrix (Fig. 5E). In comparison to facies 1 the redox sensitive trace elements are increasing whereas the detrital elements show a distinct decrease.

4.3 Facies 3 – Thin-Bedded silt-rich mudstones

The coarsest facies consist of predominately silt-rich laminae (Fig. 6A&B). Macroscopical examination shows several mm- to cm-thick continuously planar laminated silt-rich and silt-dominant beds which are interbedding with rare cm-thick fine-sand, coarse-silt beds (Fig. 6B). The silt-dominant layers have erosional bases, an upward grading structure and a high content of phosphatic (fish) debris (Fig. 6A). The interbedding silt-rich beds express wavy lenticular discontinuous laminae and a higher organic matter content. In these beds, elliptical shaped aggregates filled with compacted silt are present. The aggregates have a width of c. 0.5mm and are found in concentrated layers (Fig. 6C). They are likely of an organic origin and are present in small amounts throughout the facies. Furthermore, wavy planar stringers of carbonate are present. The strings are continuous and are predominantly horizontally-oriented but also occur in discontinuous and non-horizontal form (Fig. 6D). The cleavage is similar to the bivalve carbonate of facies 2, but contrasting the strings are

Depth (m.b.s)	Ammonite zone	Lithofacies description	Facies	Clay <2 µm	Silt 2-63 µm	Biotur-bation	Visible Tasmanites	Fecal pellets	Phosphatic debris	Pyrite	$\delta^{13}C$	Visible sedimentairy OM	Brief OM description
				%	%	%	%	%	%	%	‰	%	
30.25	*H. Bifrons*	cm-thick continously homogenous silt-bearing mudstone beds	5	30	70	10	10	70	15	5	-29.35	10	Marine snow domiated with sphearcials and tasmanites
30.40	*H. Bifrons*	Pelleted mm-thick interbedded silt-rich and clay-rich mudstone	5	30	70	10	10	70	15	5	-29.35	15	Marine snow domiated with sphearcials and tasmanites
30.88	*H. Bifrons*	Pelleted mm-thick interbedded silt-rich and clay-rich mudstone	5	25	75	10	10	70	15	5	-28.99	15	Marine snow domiated with sphearcials and tasmanites
31.48	*H. Bifrons*	wavy planar bivalve-rich pelleted mudstone	5	20	80	<1	10	15	10	5	-29.32	10	Marine snow domiated with sphearcials and tasmanites
33.80	*H. Falciferum*	Pelleted mm-thick interbedded silt-bearing clay-rich mudstone beds	4	20	80	<5	15	50	10	5	-29.26	30	Marine snow dominated with Tasmanites
34.37	*H. Falciferum*	Homogenous pelleted clay-rich mudstone	4	20	80	<1	15	50	7.5	5	-28.95	40	Marine snow dominated with Tasmanites
34.62	*H. Falciferum*	Pelleted mm-thick interbedded silt-bearing clay-rich mudstone beds	4	20	80	<1	15	60	10	5	-28.82	40	Marine snow dominated with Tasmanites
35.33	*H. Falciferum*	Pelleted mm-thick interbedded silt-bearing clay-rich mudstone beds	4	20	80	<1	15	20	10	5	-28.69	40	Marine snow dominated with Tasmanites
37.28	*H. Falciferum*	Homogenous pelleted clay-rich mudstone	4	20	80	<1	5	30	5	5	-28.70	45	Marine snow dominated with Tasmanites and sphearicals
39.95	*H. Falciferum*	Interbedded silt-rich mudstone	3	40	60	5	<5	5	5	5	-26.43	15	Marine snow dominated with single, small, sphearicals
40.72	*H. Falciferum*	Interbedded silt-rich mudstone	3	40	60	5	<5	5	5	5	-29.91	15	Marine snow dominated with single, small, sphearicals
42.31	*H. Falciferum*	clay-rich, silt-bearing mudstone	2	20	80	<1	<1	<5	<5	5	-32.82	50	Marine snow dominated with clusted sphearicals
43.09	*D. Tenuicostatum*	Bioturbated, upward graded, pyrite-rich silt-dominand mudstone	1	30	70	15	<1	<1	<1	15	-25.98	5	Pollen and spore dominated OM with dinoflagelates and achritarcs
43.96	*D. Tenuicostatum*	Bioturbated, upward graded, pyrite-rich silt-dominand mudstone	1	30	70	20	<1	<1	<1	15	-25.68	5	Pollen and spore dominated OM with dinoflagelates and achritarcs
45.14	*D. Tenuicostatum*	Bioturbated, upward graded, pyrite-rich silt-dominand mudstone	1	40	60	20	<1	<1	<1	15	-25.79	5	Pollen and spore dominated OM with dinoflagelates and achritarcs

TABLE 1 Summary of the studied thin sections of the Schandelah Core. From left to right: Depth (mbs), zone, lithofacies description, facies, grain-size, observed structures and carbon isotope values.

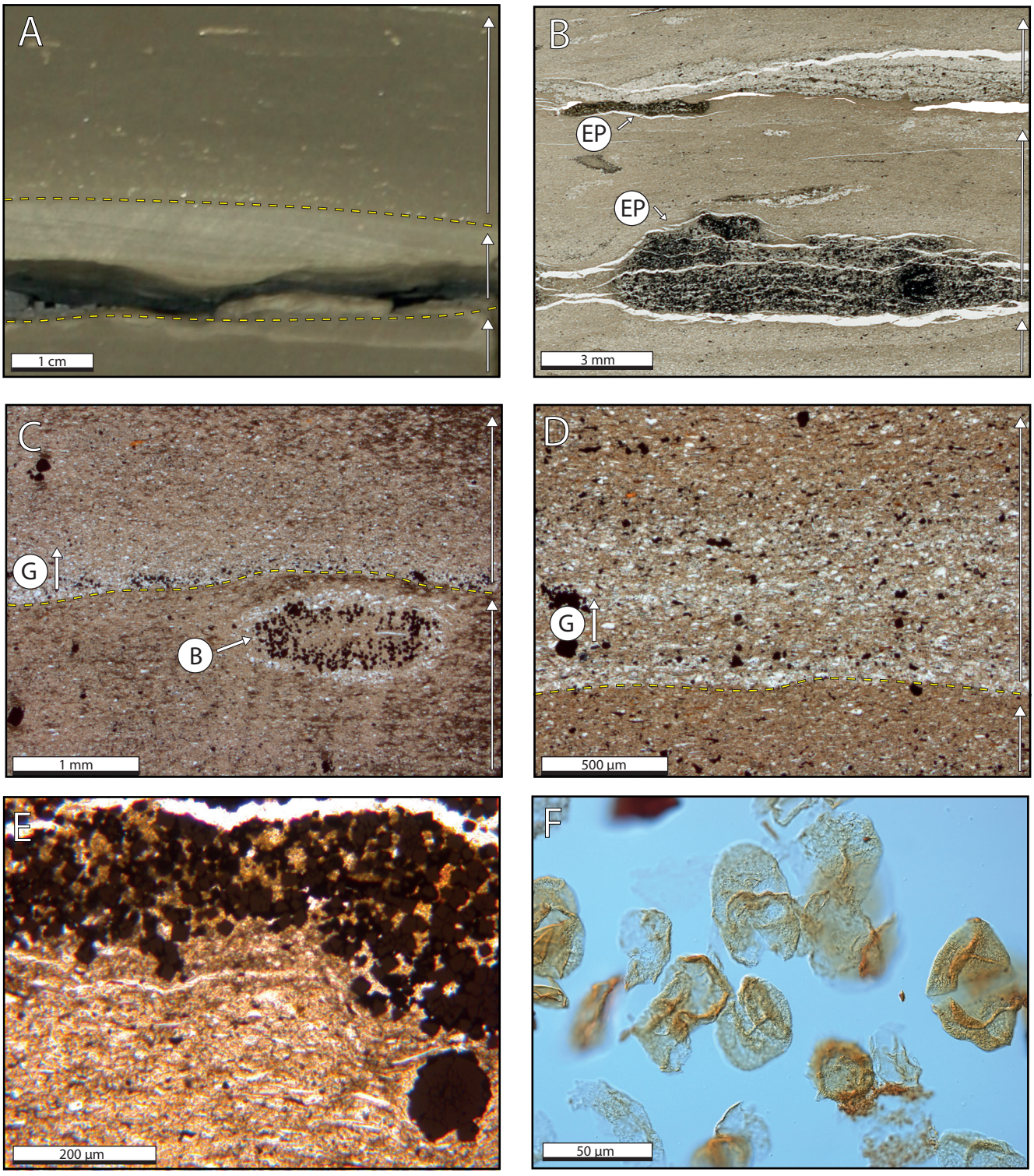

FIG. 4 A plate showing the characteristics of facies 1 A) Core photo (44.53 mbs) of a cm-thick sand bed with a continuous parallel downlapping laminae between two several cm-thick homogenized bioturbated beds. B) Optical micrograph (43.09 mbs) displaying two beds of reworked euhedral pyrite (EP). The top bed forms the base of a successive upwards grading sequence. C) Optical micrograph (43.96 mbs) of two successive upward graded beds with the top bed showing an erosive base. In the top of the first sequence a pyrite and silt filled burrow (B) can be recognized, indicating that material from the second sequence was moved down. D) Optical micrograph (45.14 mbfs) of an upward grading bed of coarse silt up to clay minerals, all well sorted. E) Optical micrograph (45.14 mbfs) showing a close up of a pyrite bed showing a squared and edged shape of the pyrite crystals indicating euhedral pyrite. F) Optical micrograph (44.00 mbfs) of degraded pollen and spore material which contributes to the majority of the organic matter composition of the facies.

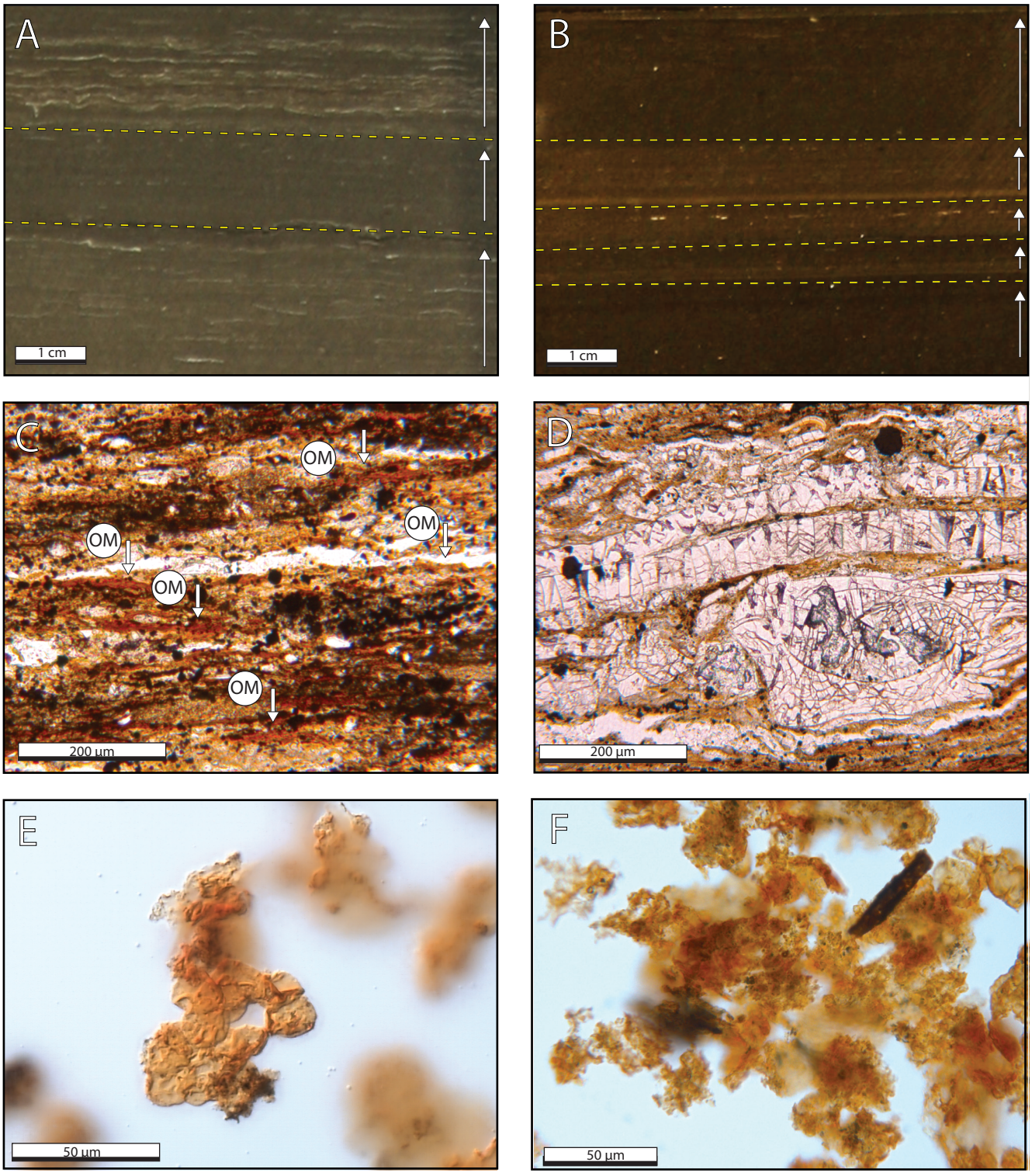

FIG. 5 A plate showing the characteristics of facies 2 A) Core photograph (42.15 mbfs) showing two beds of packed shell pavements from bivalves indicating short-term benthic colonization between the normal clay dominated background sedimentation. B) Core photograph (42.55 mbfs) of cm- to mm-thin planar laminated clay and ne-silt beds makes up the majority of the second facies. C) Optical micrograph (42.31 mbs) showing abundant drapes of orange organic matter (OM) between the silt partials and clay minerals. The beds are very homogenous. D) Optical micrograph (42.31 mbs) of a shell pavement showing clear biogenic carbonate structures and compressed shell material. E) Optical micrograph (42.50 mbs) of A small clustered group of sphaericals with at the top a small particle of marine snow attached. F) Optical micrograph (42.50 mbs) of displaying the amorphic organic matter of marine snow dominates the organic matter content of facies 2. In the top right of the image a small opaque wood fragment is recognized.

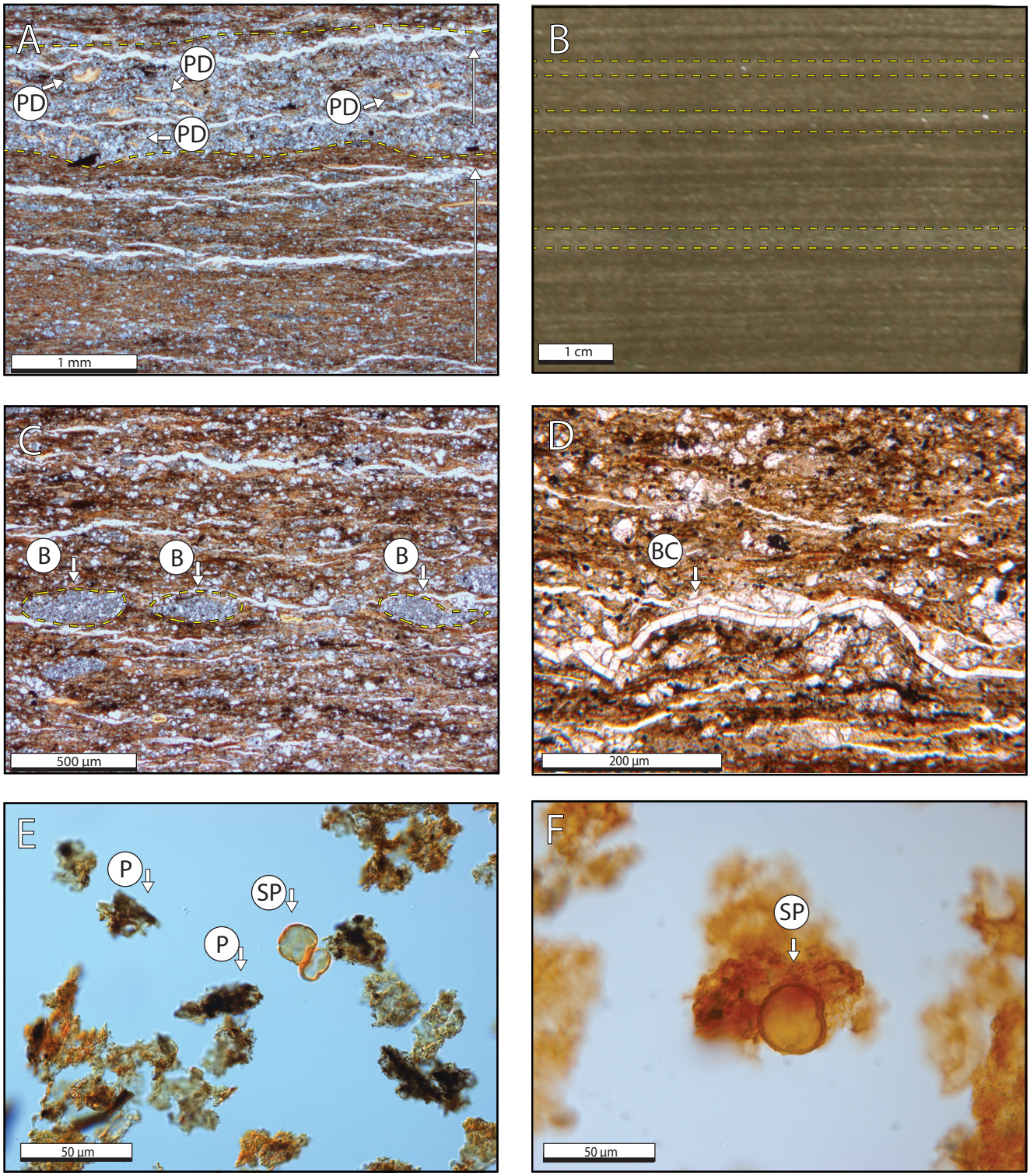

FIG. 6 A plate showing the characteristics of facies 3 A) Optical micrograph (40.72 mbs) of a coarser silt-dominated bed with an erosive base. Inside the bed a high concentration of phosphatic fish debris is concentrated indicating the possible reworking of material and a high energetic environment. B) Core photograph (40.30 mbfs) of planar continuously several mm- to cm-thick laminated silt-rich and silt-dominant beds who are interbedding with clay-rich beds. C) Optical micrograph (39.95 mbs) showing elliptical shaped lenses filled with compacted silt which are interpreted as bioturbation. D) Optical micrograph (39.95 mbs) of a single wavy biogenic carbonate string of likely bivalve origin. E) Optical micrograph (40.40 mbs) of two sphearicals. Besides the sphaericals the pyrite content in the marine snow is substantially high. F) Optical micrograph (40.00 mbs) of a single sphearical covered by marine snow.

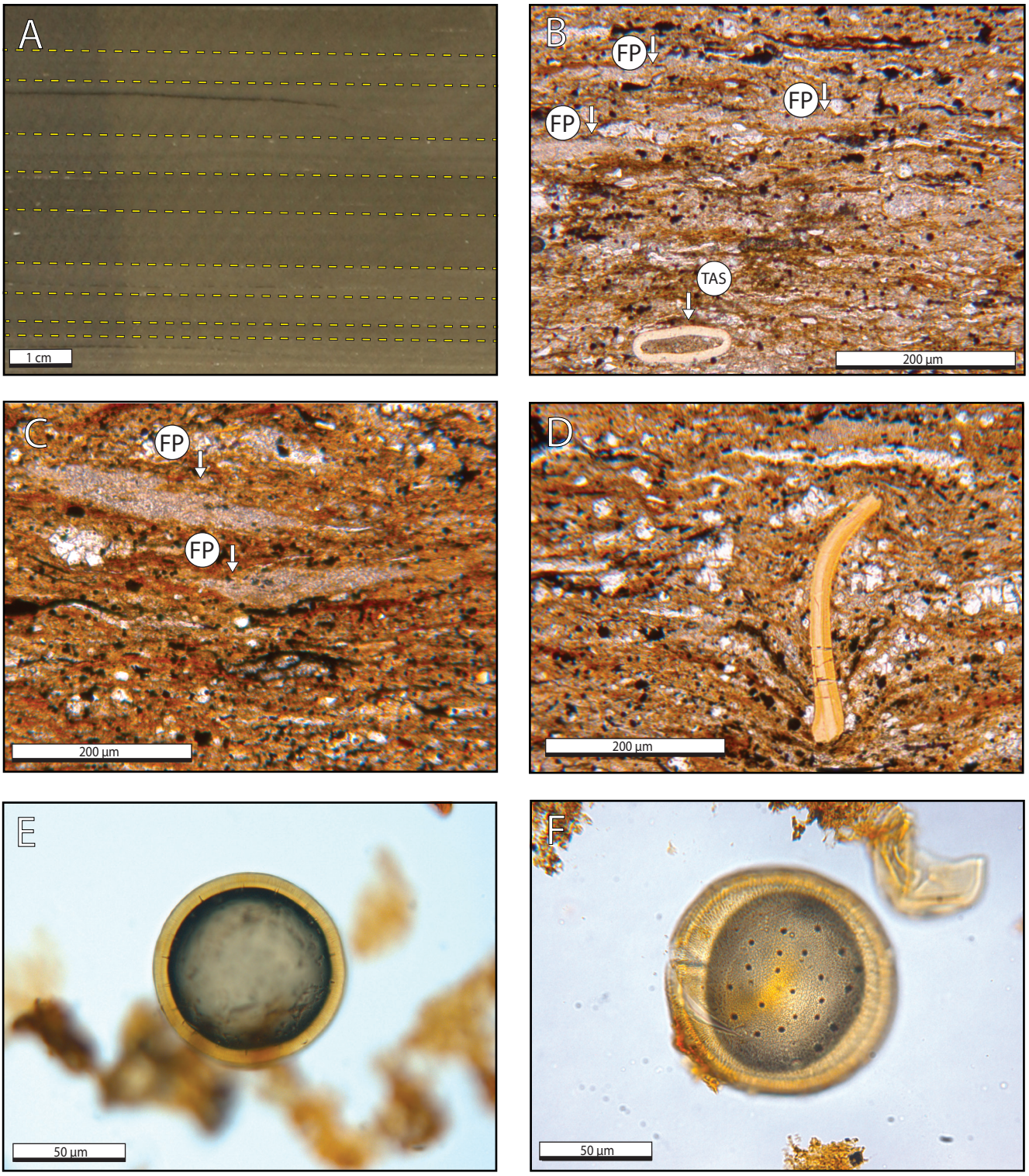

FIG. 7 A plate showing the characteristics of facies 4 A) Core photograph (36.15 mbs) of cm-thick interbedding of clay-rich and clay-dominant beds. B) Optical micrograph (34.62 mbs) of abundant faecal pellets (FP) in the matrix. In the bottom left corner, a compressed *Tasmanites* remain is visible. C) Optical micrograph (37.28 mbs) showing two faecal pellets (FP). They are of light grey colour and show a compressed elliptical shape with wispy edges. D) Optical micrograph (35.33 mbs) of a phosphatized fish bone which has fallen into the sediment. The orientation and surrounding lamination indicate the surface sediment was a gooey layer. E) Optical micrograph (36.50 mbs) of a the *Tasmanites* palynomorph, *Tasmanites* sp. 1 (*Tasmanites normales*) F) Optical micrograph (36.50 mbs) of a the *Tasmanites* palynomorph, *Tasmanites* sp. 2 (*Tasmanites punctalis*) were the outer cell wall is punctuated.

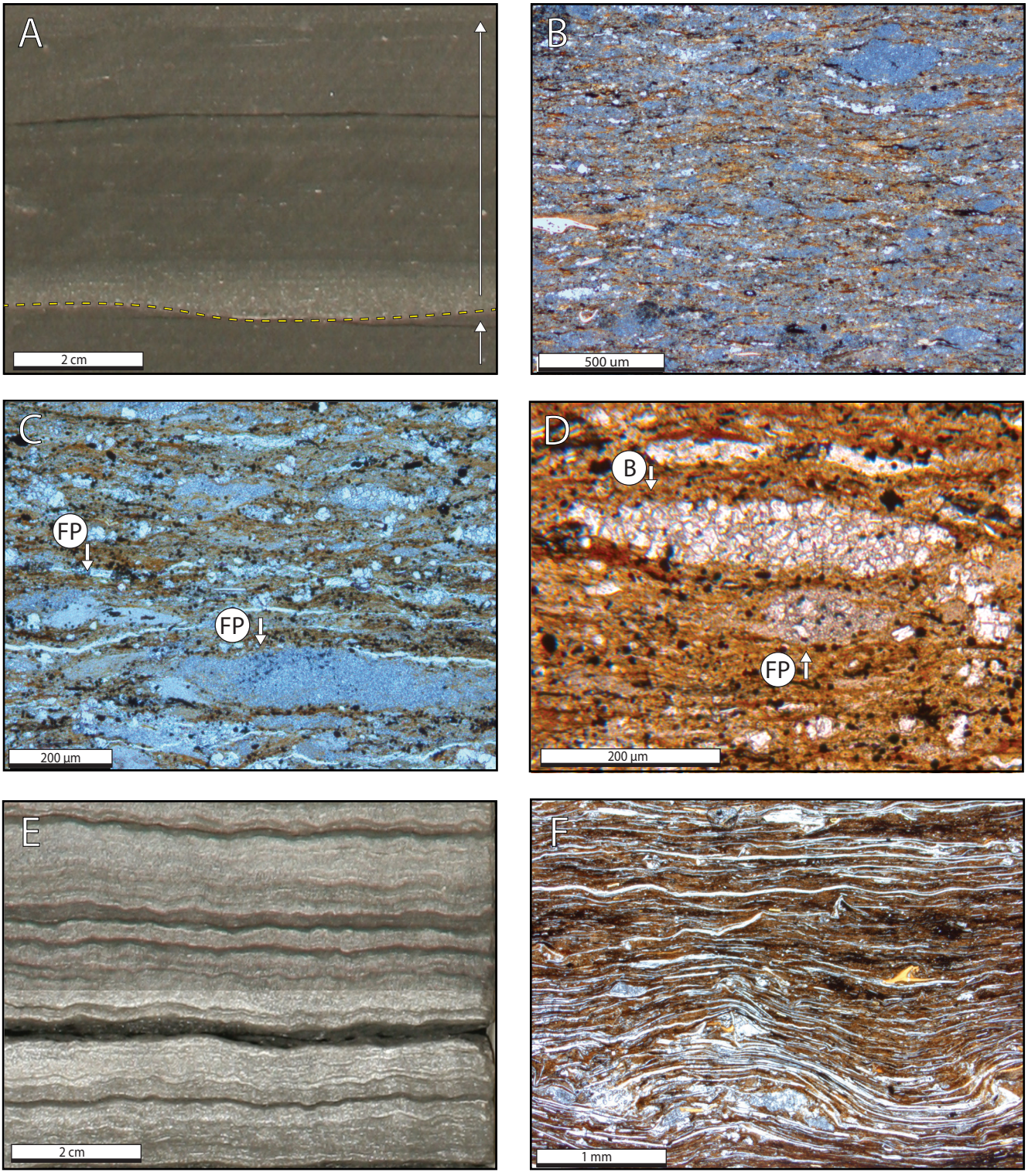

FIG. 8 A plate showing the characteristics of facies 4 A) Core photograph (30.35 mbs) of two successions. The second successions show an upwards grading sand bed with an erosive base. B) Optical micrograph (30.80 mbs) of a faecal pellet rich bed. The pellets are matrix forming and larger in size than facies 2. C) Optical micrograph (30.80 mbs) showing a close up of the faecal pellets (FP) in the enriched bed. D) Optical micrograph (30.40 mbs) of an ellipse shaped silt lens interpreted as bioturbation or the remains of an agglutinated foraminifera (B). Below this lens a small faecal pellet is situated (FP). E) Core photograph (31.40 mbfs) of the Monotis bank showing distinct curvy laminated beds. F) Optical micrograph (31.48 mbs) of the Monotis bank showing thin stacked and wavy carbonate strings origination to the benthic colonisation of bivalves. Between these strings phosphatic fish debris, faecal pellets and silt grains are trapped.

thinner. Secondly the strings are not only concentrated in beds but also present in single form. The carbonate strings are interpreted as a bivalve material from a different species. The pyrite content of this facies is framboidal and similar to the bituminous facies. The visible organic matter content is lower than facies 2, but still a high amount is preserved in the rock record. The organic matter is dominated by marine snow and has a high content of pyrite captured inside (Fig. 6E). Besides the marine snow sphaericals are still the majority of palynomorphs seen. However, the sphaericals are primarily present is single, slightly larger form (median of 25 µm) and the clustering is reduced (Fig. 6F). Besides the sphaericals occasionally larger prasinophytes, Tasmanites, are observed. In low amounts pollen and spores can be found. The geochemical analysis points out that the decrease in detrital elements of facies 2 continuous. Furthermore, a drop in redox the sensitive elements can be observed.

4.4 Facies 4 – Thin-bedded pellet- and algae-rich clay-rich mudstone

The fourth facies is clay dominated and shows an interbedding of clay-rich and clay-dominant beds (Fig. 7A). In low occurrence, more silt enriched mm-thick interlaminating beds are recognized. These beds have a lower occurrence than similar beds of the second facies. The overall lamination of the beds is planar and continuous, however occasionally wavy laminae are present. Individual beds are typically sharp based and defined by discontinuous silt lags. Thin section analysis shows that the individual beds consist of wavy laminae. Furthermore, pelleted aggregates are present. They are of light grey colour and show a compressed elliptical shape with wispy edges. Inside the pellet matrix rounded shapes can be observed. The pellet content is substantially high throughout the whole facies. With several mm intervals, the pellets are abundant to matrix forming (Fig. 7B&C). The pyrite content, framboidal, is similar to facies 2 and 3. Phosphatic (fish) bone debris is present in relative high amounts (Fig. 7D). The visible organic matter in thin section is relatively high but not exceeding the bituminous facies 2. The organic matter content consists of primarily marine snow but unlike the other facies the content of palynomorphs is higher. The most dominant palynomorphs are the prasinophytes group. Unlike facies 2 and 3, instead of the sphaericals palynomorphs, the Tasmanites genus is prevailing. With their circular shapes and flexible but strong outer wall they are not only visible in the palynological slides but also in the thin section as compressed elongated shapes (Fig. 7B). Two different palynomorphs of the Tasmanites genus are defined. Tasmanites sp. 1 (*Tasmanites* normales) where the outer membrane forms a smooth surface (Fig. 7E) and Tasmanites sp. 2 (*Tasmanites* punctalis), where the outer cell wall is punctuated (Fig. 7F). Both the genera have a larger diameter (median of 35 µm) then the previously observed sphaericals. Besides Prasinophytes, an occasionally light increase in pollen (predominantly *Classopollis* spp.) is observed. The trace element data peaks in facies 4 reaching the highest values during the entire interval. The detrital elements show a continuation in the decrease of Al and Ni.

4.5 Facies 5 – Pellet-rich bioturbated silt- and clay-bearing mudstone

This facies consists of silt- and clay-bearing mudstones. Macroscopically cm- to mm-thick planar continuous silt-rich and clay-rich laminations are dominant. Some of the laminations are discontinuous or truncated. Occasionally cm-tick coarse-silt, fine-sand beds are interbedding the common lamination. These beds have basal scour marks and form erosive bases (Fig. 8A). Shell pavement layers over cm-thickness are present. Like facies 4 the pellet content is high and some layers they form the majority of the layer content. However, the size and colour is aberrant (Fig. 8B&C). Whole beds of pellets are present at several mm-scale. Besides pellets coarse shaped elongated silt aggregates, similar to facies 3, are recognized (Fig. 8D). They occur in horizontal beds and with a higher frequency than within facies 3. The organic matter content is lower than facies 2 and 4 and the content is still dominated by marine snow. Besides the marine snow the prasinophytes are the most common palynomorphs. The trace element data implies that the decreasing trend of detrital elements stagnates in facies 5. The redox sensitive elements point out a decrease in facies 5 in comparison to facies 4.

4.6 Monotis bank

The start of the *H. Bifrons* zone is marked by a carbonate-rich bed which macroscopically displays wavy lamination (Fig. 8E). Several, interlaminated mm- to cm-thick light and dark grey beds can be recognized. In thin section the beds are similar to the biogenic carbonate strings in facies 3. Thin, wavy carbonate strings form the matrix of the bank (Fig. 8F) and the interbedding colour pattern bed is due to the density of these strings. In between the strings phosphatic debris, faecal pellets, and Tasmanites are entrapped. Besides organic materials, silt entrapped rich beds are distinguished. The origin of these organic carbonates is most likely bivalve and some authors suggest they represent the genus *Pseudomytiloides dubius* (Röhl et al., 2005; Morten et al., 2009).

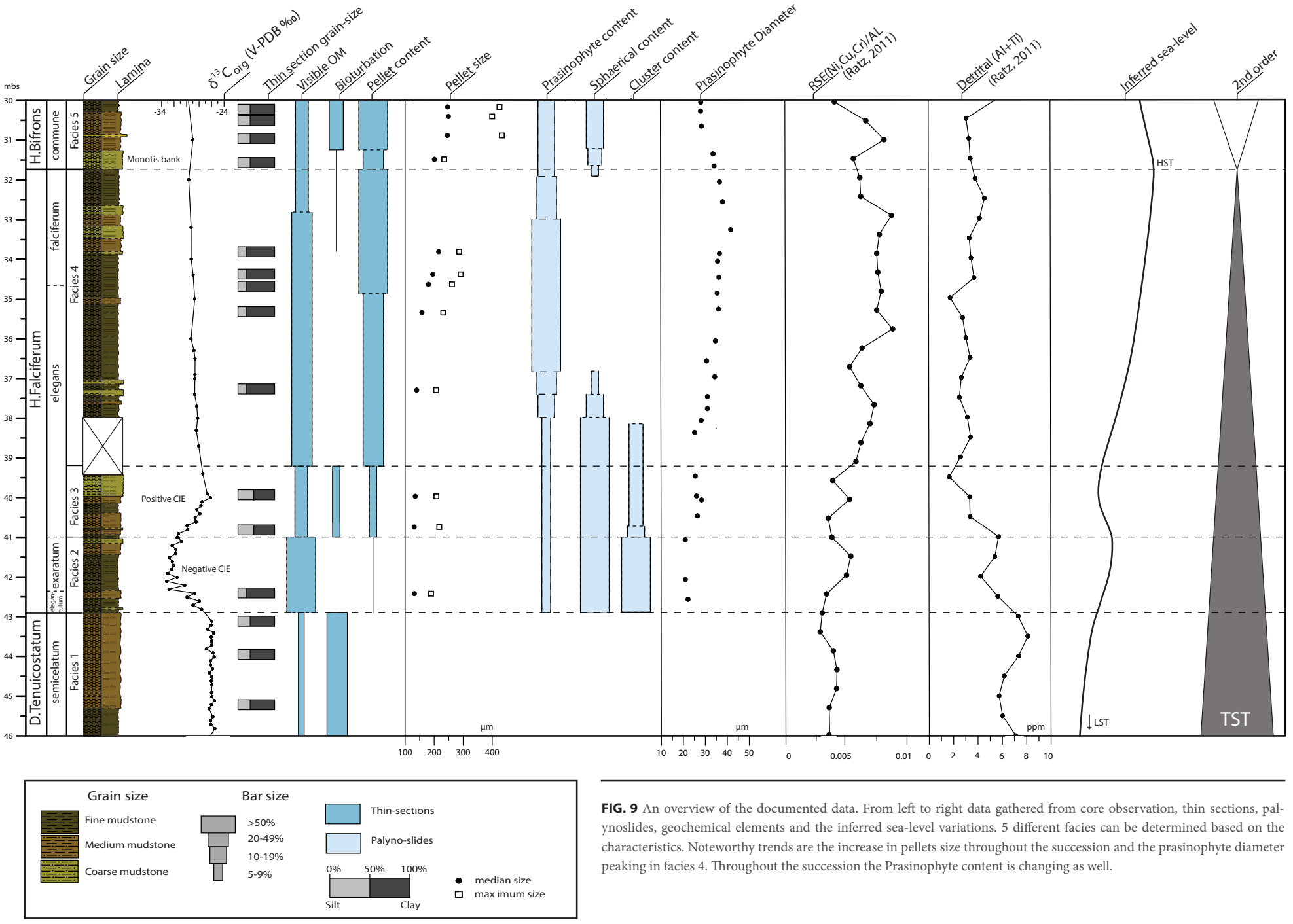

FIG. 9 An overview of the documented data. From left to right data gathered from core observation, thin sections, palynoslides, geochemical elements and the inferred sea-level variations. 5 different facies can be determined based on the characteristics. Noteworthy trends are the increase in pellets size throughout the succession and the prasinophyte diameter peaking in facies 4. Throughout the succession the Prasinophyte content is changing as well.

5. Discussion

As already noted, the entire interval can be divided into a four-component system of carbonate, pyrite, organic matter and siliciclastic material. The provenance of these components has different origins and delivering the components to the location can be done via different mechanisms. Carbonate, pyrite and organic matter are autochthonous derived components forming in the overlying water column or in the sediment itself. The forth component, siliciclastic material, has an allochthonous origin and can be deposited in several ways.

5.1 Sediment delivery and deposition

Several reconstructions of the German Basin indicate that the study site is likely to have been located in a far offshore position (e.g. Röhl et al., 2005; Song et al., 2015). In general, the succession is dominated by fine-grained silt and clay. The absence of sand sized grains correlates with depositional sites on the mid to far shelf (e.g. Macquaker et al., 2007; Plint 2010; Plint et al., 2012; Trabucho-Alexandre et al., 2012) and aid the proposed offshore provenance. However, based on the fact that the texture, fabric and composition of the facies are entirely different, the transport of the silt and mud must have been facilitated by different processes.

The first facies is marked by upward graded beds and erosional bases. A possible explanation for such depositional structures is the transport of the sediment by oscillatory wave action (Plint, 2010). However, the absence of wave and combined flow ripples in the facies doubts this depositional mechanism (Schieber, 1990). This absence also carries the implication that the depositional depth is beneath 50 meters, below the reach of oscillatory wave action. Nevertheless, the observed scour marks and graded bedding suggest high-energy events occurred periodically during the deposition of the facies. Combined with the euhedral pyrite beds (Fig. 4B), indicating input of reworked marine sediment (Schieber et al., 2011), a likely explanation for these structures is storm induced deposition of hyperpycnal flows (Schieber, 1990; Aplin et al; 2011). Facies one can thus be described as an episodically energetic, depositional site which is most likely located in a midshore position.

The second facies is characterized by the start of black shale deposition, as is evidenced by the increase in visible organic matter (Table 1). Besides the difference in organic matter content a change in sedimentological structures also suggest a change in the sea-level of the basin. The absence of euhedral pyrite, erosive bases and graded bedding leads to the assumption of a shift in depositional style towards a lower energetic environment. The most likely explanation for this decline in energy is an increase in sea-level, locating the studied site at a more distal, lower energetic position. This change is well captured by the decrease in grain-size (Fig. 8; Table 1) and the loss of detrital elements. Land-derived elements that track the input of terrigenous input (Al, Ti) decrease steadily during the second facies (Fig. 9). Due to the proposed far offshore position and the relatively low depositional reach of storm endured deposits (Schieber, 2016) it is unlikely that the observed sedimentological structures are created by storm energy. With the storm induced deposition ruled out, turbidite flows are the most likely depositional mechanism during these facies (Schieber, 2016). In present-day environments turbidite flows have a large range of deposition and are an important mechanism for far offshore deposition. Nonetheless, to generate a classical turbidite a larger slope (>0.5) is needed then assumed for the epicontinental shelf (in the range of 0.01 to 0.001) (Aplin et al., 2011; Schieber, 2016). However, as hypothesized by Macquaker et al. (2001) surficial sediments deposited by hyperpycnal mechanism could be remobilized and transported further offshore as gravity flows if they are aided by storms. The range of this deliverance mechanism can be up to 400 km offshore (Schieber, 2016). Facies two can thus be interpreted as the start of a sea-level rise as indicated by a major change in depositional style. The studied site moves towards a more distal, offshore, position.

The third facies, again, displays a shift in depositional style. The increase is silt sized particles (Fig.9; Table 1) combined with the reoccurrence of erosional bases and graded silt beds suggest a similar setting as facies 1. The high concentration of phosphatic fish debris in the coarsest silt beds (Fig. 6A) aid this hypothesis. The concentrated occurrence could indicate the reworking of marine material, similar to the euhedral pyrite beds. Furthermore, the scatter orientation of the biogenic carbonate strings (Fig. 6D) suggests a higher energetic environment at the sediment-water interface compared to the planar orientated biogenic carbonate of facies 2 (Fig. 5D). All these observations point towards a more energetic, possibly storm induced, deposition. This implies a decline is sea-level during the third facies leading to a more proximal position and the above the storm wave base.

The successive forth facies has similar characteristics to facies two. However, in comparison to the second facies, the lesser presence of silt layers may indicate that the depositional setting of the site was more distal than facies two. This suggest a continuation of the sea-level rise started during the second facies. Therefore, facies 3 can be interpreted as a small, 3th order, sea-level decrease. The zenith of the increase in sea-level is reached at the Monotis Bank. The organic carbon enriched Monotis bank is linked to a maximum flooding surface. An increasing distal position ultimately will lead to lack of terrigenous material and a lowered sedimentation rate, resulting into a condensed section (e.g. Loutit et al., 1988; Wignall,

1991a; Macquaker and Jones, 2002). The high concentration of pelagic-fossils (Fig. 8E&F) in the Monotis Bank aids this observation. Due to the starvation of terrigenous input, pelagic-fossils where able to develop in abundancy at this site (e.g. Haq et al., 1988).

The last facies is characterized by an increase in grain size (Fig. 9, Table 1). This increase in combination with the occasional presence of scour marks leads to the assumption that the sediment delivery is becoming more energetic. Facies 5 therefore, can be interpreted as the start of a regressional movement.

The observed trends in sea-level variation lead to an inferred, 3th order, sea-level curve shown in figure 9 and 10. The suggested curve is in good alignment with previously constructed sea-level curves (e.g. Röhl et al., 2005) and the assumed second order transgressional movement during this period. (Haq et al., 1988; Hallam et al., 2001)

5.2 Organic matter characteristics

The visible organic matter content suggests that the episodes with the highest enhancement of organic matter deposition are facies 2 and 4 (Table 1). The organic matter that ultimately reaches the sediment and is captured in the rock record originates from three primary sources: pellets, prasinophyte algae and marine snow. While the marine snow does not fluctuate greatly the other two components vary throughout the different facies. The observed pellets display an increasing trend in abundancy and size throughout the successive facies. At their first occurrence in facies 2 the abundancy and size (median c. 130 µm, maximum c. 200 µm; Fig. 9) is relatively minor. During facies 4 and 5 the pellets are characterized by a higher abundancy as well as an increased size (median c.250 µm, maximum c. 430 µm; Fig. 9). A similar trend is visible for the prasinophyte group. During the second facies, the green algae diameter is relatively small (median c.20 µm; Fig. 9) as in the later facies 4 the size increases (median c.20 µm, maximum 100 µm; Fig. 9). Unlike the pellets, the subsequent fifth facies is marked by a decrease in size (Fig. 9). The clear shifts in size as well as abundancy of the different components could be used as proxy for changes in the water column. In the following paragraphs the origin and implications of the different organic matter components will be discussed.

5.2.1 Pellet origin

The origin of the pellets is likely to be organic and represents the faecal products of organisms. The relative absence of pyrite in the pellets (Fig. 7B&C; Fig. 8B&C) suggests that the internal microchemistry was slightly different than that of the surrounding matrix. A possible explanation for this absence could be that the available iron (which is needed for the formation of pyrite) was removed prior to the burial by the digestion of the producing organism (Macquaker et al., 2010). Another possibility is that the permeability inside the faecal aggregate was not large enough to make organic matter, sulphate, and iron react with each other. In addition, round shapes are visible in the pellets (Fig 7C). These could be phytoplankton debris such as coccolithophore skeletons. Pellets with this composition are commonly found in black shales and are most likely produced by zooplankton (e.g. Macquaker et al., 2010; Plint et al., 2012; Hart et al., 2013). There are no clear indications for pellet production at the sediment water interface during facies 4. With the absence of trace fossils, faecal pellet mounds (Wild et al., 2005) and the horizontal pellet orientation the production is most likely to originate from the water column. The relatively small size of the faecal pellets is an additional indicator of a zooplanktonic origin and thus production in the water column (Turner et al., 2002). The preservation of large amounts of faecal pellets classically is linked to the presence of anoxic bottom water conditions (Pilskaln et al., 1987; Turner et al., 2002). However, an abundance of faecal pellets may also counteract burial and sulfurization in sediment layers leading to a better preservation of the organic matter (Sinninghe Damsté et al., 1998).

Thus, although full anoxic conditions enhance the preservation of organic matter the abundance of faecal pellets may be an enhancement for preservation on its own. Some authors suggest that the faecal pellets could be moved via hyperpycnal flows (Cuomo and Roads, 1987; Lash, 2016) but the high abundancy, planar pellet orientation (Fig. 6B&C) and absence of real beds in facies 4 suggest it is likely to be an in-situ production. The increasing faecal pellet size observed during the fifth facies leads to the assumption that larger organisms were able to survive in the water column. In facies 5 the beds of pellets insinuate episodes of enhanced biological activity. Besides the size, the pellets have a more ellipsoid shaped morphology. This could indicate a different composition of the faecal pellets with a higher strength. It is possible that these pellet beds envision benthic activity.

5.2.2 Prasinophytes

Prasinophyte green algae have been recorded in Early Toarcian strata throughout Europe and at the Schandelah site they form a prominent component of the organic matter. Besides large Tasmanites, the small sphaericals (or sphaeromorphs in some literature) are recorded in the different Early Toarcian black shales as well (Prauss et al., 1991; Bucefalo Palliani et al., 2002). The occurrence of these sphaericals is regularly associated with the Tasmanites genus but besides this correlation not much is known of the sphaerical origin. Present day prasinophycean green algae can provide a valuable inside into this matter. The life cycle of these prasinophytes (genus *Ptemosperma)* can be divided into two phases, a juvenile and an adult phase. In the juvenile stage the algae

form small (c. 20 µm; Boalch et al., 1978) non-motile cells in a nearshore environment. These juvenile algae float passively into open ocean where, within a short time period, their size and cell wand thickness increases leading them into their adult phase (Boalch et al., 1978). The relationship between the small sphaericals and the larger *Tasmanites* may be of similar origin. The morphology of the sphaericals expresses the same, rounded and resistant cell wand as observed by the *Tasmanites* (Fig. 5E&G). With this morphological likeness and the fact that the *Tasmanites* have an increased size and cell wand thickness in comparison to the sphaericals, we argue that the sphaericals palynomorphs represent the juvenile phase of *Tasmanites*.

The control on the assemblage of prasinophytes seems to be primarily driven by nutrient availability (Vigran et al., 2008). It is hypothesized that nitrogen is the ultimate cause for stimulation of prasinophyte productivity. Besides this parameter the prasinophyte population also seems to have a higher affinity with cooler water and a high tolerance for variable salinity (Prauss et al., 2007; Vigran et al., 2008).

The clustering of the sphaericals observed during the negative CIE (Fig. 9) could be another indicator of a severe stressed environment. These prasinophycean green algae reproduce asexually via fission. This means that the parent cell divides into several parts and regenerates those parts into separate entities creating new juvenile algae. Extreme stressed conditions could supress the completion of normal prasinophyte development. A similar case is seen during the end-Jurassic mass extinction. Lower Jurassic spores were regularly released in unseparated spores indicative of failure to complete the normal process of spore development (Visscher et al., 2004). The stress factor for this anomaly is attributed to increased levels of UV-radiation due to large scale volcanic activity (Van de Schootbrugge et al., 2016). With the Karoo-Ferrar large igneous province (Fig. 1A) active at the time of the Toarcian CIE (Van de Schootbrugge et al., 2013 and references herein) the clustered sphaericals could have a similar origin as the unseparated spores.

5.2.3 Marine snow

The last and dominant component of the organic matter is marine snow. In the water column, much of the suspended material that that is larger in size than a few microns exist as aggregates of organic-derived debris. This debris has different sources such as zooplankton, phytoplankton, micro-organisms, but also bacteria and faecal pellets as well as silt and clay (e.g. Macquaker et al., 2010; Alpin et al., 2011; Turner et al., 2015). Aggregates are abundant in the marine pelagic zone and the aggregation causes a high settling rate (e.g. Kranck et al., 1980). A "glue" of mucopolysaccharide substances secreted by marine plankton causes the particles to aggregate together (Macquaker et al., 2010 and references herein). Marine snow in the present-day is most abundant below areas with enhanced primary production and large phytoplankton blooms.

5.2.4 In-situ fauna

Besides organic components originating from the water column there is also evidence for the production at the sediment-water interface. The distinct silt lenses of facies 3 and 5 (Fig. 7D) are most likely burrowed structures of unknown origin (e.g. Röhl et al., 2005; Macquaker et al., 2010). Another possible origin for some of these lenses are the remains of agglutinated foraminifera. There are several examples from black shales where similar sized and shaped lenses are observed and attributed to a benthic foraminiferal origin (e.g. Schieber et al., 2009; Macquaker et al; 2010, Plint et al; 2012). Either of these two possible options advocates that long-term persistent anoxia cannot have existed throughout deposition of these facies and that benthic colonization was present.

The short intervals of biogenic carbonate in facies 2 and 3 represent opportunistic recolonizations of the seafloor after a short period of storm induced reoxygenation. These event communities are likely to last only a few weeks to several years on the seafloor after which anoxic conditions were re-established (Röhl et al., 2001; McArthur et al., 2008).

5.3 Towards a revised depositional model

On the basis of the above discussed observations a revised depositional model for the Early Toarcian black shales in the North German Basin can be constructed, thereby testing the two favoured models for the enhanced organic matter deposition (Salinity stratification and basin restriction, Fig. 2A&B). Changes in sediment delivery mechanisms as well as organic matter content suggest that the entire interval is more heterogeneous and dynamic than formerly supposed. The distinguished facies of this study imply temporal changes in the style of deposition of the organic matter. Based on these temporal changes a new, refined, model for the North German Basin is shown in figure 10.

5.3.1 Pre-black shale environment

The *D. tenuicostatum* presents a pre-depositional phase (Fig. 10A). With a relative lowstand in the sea-level during the first facies, wave induced mixing of the water column lead to oxygenated bottom waters around the entire basin. This well oxygenated environment is illustrated by bioturbation of the sediment and the abundance of spores, pollen, dinoflagellates and acritarchs.

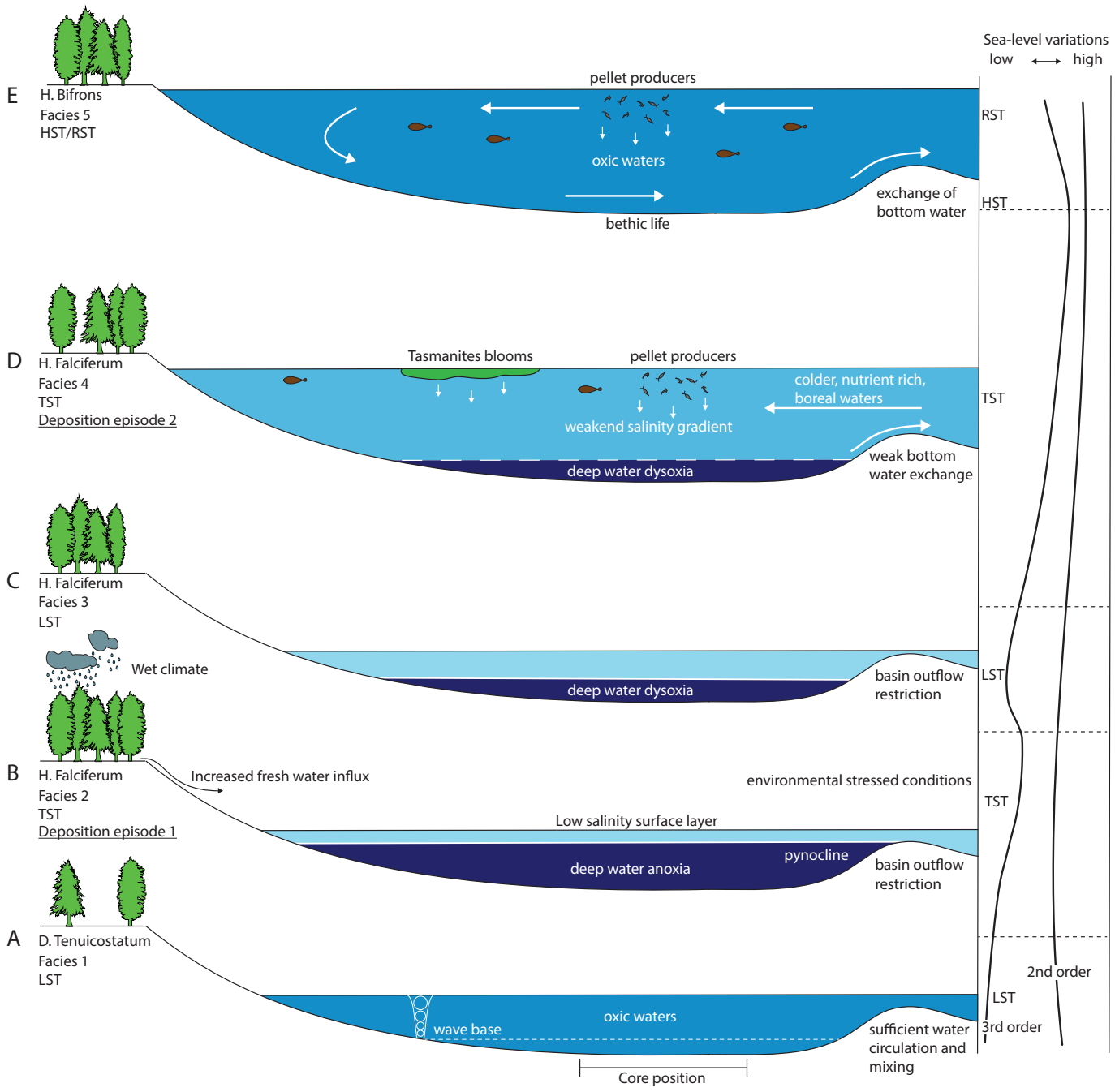

FIG. 10 An overview of the different episodes of black shale deposition. Starting at a with a lowstand in the *D.Tenuicostatum* zone there is a complete exchange with other basins and a well-mixed water column. The subsequent early transgression during the exaratum aligns with a warm, wet climate and high runoff of fresh water leading to salinity driven stratification which is enhanced by basin restriction. A third order regressional phase leads to wind and water mixing and dysoxic deep waters only the deep part of the basin. With the continuation of the transgression a shift in black shale deposition style occurs. Inflow of colder, nutrient-rich, boreal waters lead to a productivity driven black shale sedimentation while maintaining a weakened salinity gradient. Reaching a sea-level highstand the dysoxic conditions are lifted and reoxygenation of the bottom water is manifested.

5.3.2 Preservation driven deposition

The deposition of black shales starts during the second facies 2 (Fig. 10B). In the elegantulum and exaratum subzone of the *H.falciferum* a drastic change in sedimentation occurs. Facies 2, the first facies with a high organic matter content, aligns with the global negative CIE (Table 1; Fig. 9). This perturbation of the carbon cycle would have had a strong impact on the environmental conditions (Van de Schootbrugge et al., 2013; Suan et al., 2015). It is argued that the already tropic environment developed into an even warmer and wetter climate due to greenhouse intensification (Jenkyns, 2003). As a consequence of this climate intensification, runoff of freshwater into the oceans became substantially high. High levels of osmium isotopes and lighter oxygen isotope values indicate this increase in runoff for the northern European basins (Cohen et al., 2004; Hermoso et al., 2014; Percival et al., 2016). With the increase of freshwater, stratification of the water column and a high pycnocline could be achieved (Fig. 10B). Besides the stratification, the low-salinity surface layer would drastically alter the living conditions for the marine organisms (van de Schootbrugge et al., 2005). This impacted is evidenced by the biological components in facies 2. With a low content of phosphatic debris, faecal pellets and besides the dominant marine snow, only clustered sphaericals in the organic matter, the link with stressed conditions can easily be made. The idea arises that the water column conditions would have been unhospitable and not able to fully support abundant large life forms. Prasinophytes, which have the reputation to well adapt and be able to survive unhospitable conditions (Prauss et al., 2008) even show deviation from their regular life cycle. The endurance of these, although stressed, sphaericals may be because of increased nitrogen in the water due to denitrification (Jenkyns et al., 2001).

However, favouring a regional concept and the absence of global black shale deposition, an increased runoff leading to a low-salinity cap could not entirely explain the enhanced black shale deposition. At the same time of the perturbation the sea-level in the North German Basin is still relatively low. As is evidenced by the microstratigraphic analysis facies 2 represent an early transgressive sea-level movement. This still relative low sea-level in the basin could have enabled the expression of the anoxia by means of basin restriction. Due to the still relative low sea-level the low-salinity cap would have been able to act a stop on deep water exchange (Fig. 10B). McArthur et al., (2008) proofs that there is evidence for this basins restriction. The ratio between the element Molybdenum and the total organic carbon (Mo/TOC), an indicator for water mass restriction, suggest there was no exchange of bottom water between different basins throughout northern Europe. The shallow epicontinental sea setting in combination with a relative low sea-level and a low-salinity cap thus can be seen as an excellent catalyst for the development of stagnant conditions and anoxia. Although there are indications for persistent photic zone anoxia during this period (Schwark et al., 2004), event communities during the second facies (Fig. 5A&D) suggest that very brief oxygenation occurred. Within the shallow anoxic water body, organic matter degradation was restricted to a very thin oxygenated part of the photic zone, and thus occurred only to a minor extent. This lead to a preservation driven enhancement of organic matter in the sediment.

The idea of a low-salinity cap combined with basin driven restriction would implicate that the two favoured models are not entirely mutually exclusive. The two models seem to enforce each other and are likely both accountable for the black shale deposition during facies 2.

Following the preservation driven enhancement, facies 3 indicates a minor drop in sea-level and improved conditions of the water column (Fig. 10C). This change in the early elegans subzone is evidenced by the loss of clustering and increase in size from the sphaericals (Fig. 9). Another indicator for improving conditions is the low, but noticeable increase in pollen and spore material and the decrease in visible organic matter (Table 1; Appendix 2). The low amount of bioturbation of the sediment suggest that the proposed sea level fall and the consequent storm induced mixing would have led to short periods of oxygenation of the sediment water interface. Likely there was only deep water dysoxia present in the deeper parts of the basin during these facies. The sea-level drop may be linked to the positive CIE, which occur in the same time period (Fig. 9), but there is not enough to support this claim.

5.3.3 Productivity driven deposition

Following this sea-level drop, the change in sedimentation style of facies 4 suggest the continuation of the second order sea-level rise. During this period, the visible organic matter content increases again. However, the composition of organic matter significantly changes. The organic matter is not abundantly dominated by marine snow. Faecal pellets and Tasmanites form a noteworthy part of the composition. This differentiates from facies 2 in such a way that it cannot be explained by the same processes. Besides this, facies 4 also occurs above the CIE (Fig. 9) implying two different phases of successive black shale deposition. The collected data suggest that the deposition of the black shales in facies 4 is more productivity driven than the anoxia driven facies 2. The increase in phosphatic fish debris, faecal pellets and *Tasmanites* indicates the development of a more marine upper water column that supports higher and larger volumes of life. Secondly the abundancy of faecal pellet production aids the preservation of other organic matter and thus less anoxic conditions are required (Sinninghe Damsté et al., 1998). This change could be governed by the increasing relative sea-level, improving communication between the Northern German Basin and adjacent areas, thereby weakening the salinity stratification

(Fig. 10D). The affinity for cooler waters by Tasmanites and an observed thrive of the genus suggest that the improved communication also created the possibility to exchange water with the nutrient-rich and colder Boreal Sea (Bjerrum et al., 2001). These nutrient-rich waters would stimulate the productivity in the top of the water column. Secondly, although more saline, these artic waters are closer to the fresh water salinity then the water from the southern Tethys Ocean. Input from these waters would lead to a weakened but not entirely absent salinity gradient (Harazim et al., 2013). In addition, there is no evidence for full or long periods of bottom water oxygenation during the deposition of the facies. This suggest that a plume of dysoxic bottom water maintained its position at least within the deep parts of the basin, enhancing the high preservation further.

5.3.4 Uplift of the conditions

Ultimately the sea-level rise leads to the renouncing of dysoxic conditions. This is well documented in the last facies and the shift from the *H. fallciferum* into the *H. bifrons* zone. The increase in faecal pellet size and decrease of marine snow in the organic matter composition, as well as the occurrence of benthic colonization, indicate improved deep water conditions. Besides the increase of faecal pellet size, the occurrence of pellet beds and different morphology suggest different, possibly benthic, pellet producers. A decrease in the prasinophyte size and total abundancy can be interpreted as less inflow of Boreal waters, fully breaking down the salinity stratification and reoxygenation of the whole basin (Fig. 10E).

6. Conclusion

The Early Toarcian black shales of the Posidonia Shale Formation are a well-known for their enhanced organic matter deposition. Despite a large amount of research the formation underwent, there is no common consensus on environmental conditions that lead to the enhanced deposition. By observing subtle and temporal changes a new idea of the deposition is developed. The Early Toarcian black shales were deposited in a marginal and deep part of the epicontinental sea covering the Northern German Basin. Overall the sediment is fine-grained and organized in normally graded thin beds (< 10 mm thick). By analysing the sediment via thin section five facies can be distinguished. The different facies indicate changes in the depositional mechanism of the sediment as well as changes in the water column. Colonisation events show that there was no prevalence of long lasting anoxic or dysoxic conditions. This indicates that productivity must have been an important controlling factor during the entire interval.

These two episodes reflect a major change in organic matter delivery within the black shale deposition. The first episode of organic matter preservation in the exaratum subzone is enhanced by anoxic bottom water conditions and is deposited during the negative CIE. This period of greenhouse intensification lead to an enhanced riverine runoff, increasing the fresh water supply to the basin. The early transgression stage of the sea-level during this period can be seen as the perfect catalyst for promoting salinity driven stratification and photic zone anoxia via basin restriction. This lead to a preservation driven black shale deposition. In response of these conditions, the organic matter composition is characterized by stress indicating clustered sphearicals and an abundancy of marine snow. With the ongoing transgressional movement in the falciferum subzone, the basin restriction was lifted entering the second episode of black shale deposition. This second episode represents a period in which the black shale deposition is productivity driven. The thrive of the prasinophytes Tasmanites genus and the support of high volumes of pellet producing organism in the upper water column suggest an influx of cold, nutrient-rich waters from the boreal sea leading to a weakened stratification with only dysoxia present in the deeper parts of the basin. The total organic content of the sediments of the falciferum subzone may be lower than those during the exaratum subzone, however the presence of faecal pellets and Tasmanites imply the viability as a good source rock. Reaching a sea-level highstand, indications for increased benthic colonisation events and the support of larger pellet producing organism suggest a slow lift of the deep water dysoxia and reoxygenation of the basin, ending the black shale deposition.

The results presented here further underscore the importance of an integrated approach when assessing black shale deposition. We suggest that more scientist need to apply the same, integrated approach to fully evaluate the rock potential of black shales.

7. Acknowledgments

I would like to thank Bas van de Schootbrugge and Joao Trabucho-Alexandre for their guidance, helpful comments and discussions. I especially want to thank Dario Harazim for his time and effort put into this thesis. Secondly, I want to mention my fellow students from room 5.17 for the discussions and joyful time. Furthermore, I would like to thank Goethe University Frankfurt for access to the drilling core and Utrecht University for access to all her facilities needed for this research.

8. Literature

- Aberhan, M. (2001). Bivalve palaeobiogeography and the Hispanic Corridor: Time of opening and effectiveness of a proto-Atlantic seaway. Palaeogeography, Palaeoclimatology, Palaeoecology, 165(3–4), 375–394. https://doi.org/10.1016/S0031-0182(00)00172-3

- Ainsworth, R. B., Flint, S. S., & Howell, J. A. (2008). Predicting coastal depositional style; influence of basin morphology and accommodation to sediment supply ratio within a sequence stratigraphic framework. Special Publication - Society for Sedimentary Geology, 90(90), 237–263. https://doi.org/10.2110/pec.08.90.0237

- Al-Suwaidi, a., Angelozzi, G. N., Baudin, F., Damborenea, S. E., Hesselbo, S. P., Jenkyns, H. C., … Riccardi, A. C. (2010). First record of the Early Toarcian Oceanic Anocic event from the Southern Hemisphere, Nequen Basin, Argentina. Journal of the Geological Society, London, 167, 633–636. https://doi.org/10.1144/0016-76492010-025.SPECIAL

- Aplin, A. C., & Macquaker, J. H. S. (2011). Mudstone diversity: Origin and implications for source, seal, and reservoir properties in petroleum systems. AAPG Bulletin, 95(12), 2031–2059. https://doi.org/10.1306/03281110162

- Bjerrum, C. J., Surlyk, F., Callomon, J. H., & Slingerland, R. L. (2001). Numerical paleoceanographic study of the early Jurassic transcontinental Laurasian Seaway. Paleoceanography, 16(4), 390–404. https://doi.org/10.1029/2000PA000512

- Boalch, G. T., Harbour, D. S., Biologicalassociation, M., Hill, C., & Waters, R. (1978). the Genus Pterosperma Equatorial, 239–276.

- Bucefalo Palliani, R., Mattioli, E., & Riding, J. B. (2002). The response of marine phytoplankton and sedimentary organic matter to the early Toarcian (Lower Jurassic) oceanic anoxic event in northern England. Marine Micropaleontology, 46(3–4), 223–245. https://doi.org/10.1016/S0377-8398(02)00064-6

- Cohen, A. S., Coe, A. L., Harding, S. M., & Schwark, L. (2004). Osmium isotope evidence for the regulation of atmospheric CO2 by continental weathering. Geology, 32(2), 157–160. https://doi.org/10.1130/G20158.1

- Cuomo, M. C., & Rhoads, D. C. (1987). Biogenic Sedimentary Fabrics Associated with Pioneering Polychaete Assemblages: Modern and Ancient. Journal of Sedimentary Research, 57(3), 537–543. https://doi.org/10.1306/212F8B89-2B24-11D7-8648000102C1865D

- Dera, G., Pellenard, P., Neige, P., Deconinck, J. F., Pucéat, E., & Dommergues, J. L. (2009). Distribution of clay minerals in Early Jurassic Peritethyan seas: Palaeoclimatic significance inferred from multiproxy comparisons. Palaeogeography, Palaeoclimatology, Palaeoecology, 271(1–2), 39–51. https://doi.org/10.1016/j.palaeo.2008.09.010

- Dera, G., Pucéat, E., Pellenard, P., Neige, P., Delsate, D., Joachimski, M. M., … Martinez, M. (2009). Water mass exchange and variations in seawater temperature in the NW Tethys during the Early Jurassic: Evidence from neodymium and oxygen isotopes of fish teeth and belemnites. Earth and Planetary Science Letters, 286(1–2), 198–207. https://doi.org/10.1016/j.epsl.2009.06.027

- Gröcke, D. R., Hori, R. S., Trabucho-Alexandre, J., Kemp, D. B., & Schwark, L. (2011). An open ocean record of the Toarcian oceanic anoxic event. Solid Earth, 2(2), 245–257. https://doi.org/10.5194/se-2-245-2011

- Hallam, A. (2001). A review of the broad pattern of Jurassic sea-level changes and their possible causes in the light of current knowledge. Palaeogeography, Palaeoclimatology, Palaeoecology, 167(1–2), 23–37. https://doi.org/10.1016/S0031-0182(00)00229-7

- Haq, B. U., Hardenbol, J. & Vail, P. R. (1988). Mesozoic and Cenozoic Chronostratigraphy and Cycles of Sea-Level Change. Sea-Level Changes. https://doi.org/10.2110/pec.88.01.0071

- Hermoso, M., Minoletti, F., & Pellenard, P. (2013). Black shale deposition during Toarcian super-greenhouse driven by sea level. Climate of the Past, 9(6), 2703–2712. https://doi.org/10.5194/cp-9-2703-2013

- Hesselbo, S. P., Gröcke, D. R., Jenkyns, H. C., Bjerrum, C. J., Farrimond, P., Morgans Bell, H. S., & Green, O. R. (2000). Massive dissociation of gas hydrate during a Jurassic oceanic anoxic\nevent. Nature, 406(6794), 392–395. https://doi.org/10.1038/35019044

- Immenhauser, A., Schreurs, G., Peters, T., Matter, A., Hauser, M., & Dumitrica, P. (1998). Stratigraphy, Sedimentology and Depositional Environments Of the Permian to Uppermost Cretaceous Batain Group, Eastern-Oman. Eclogae Geologicae Helvetiae, 91, 217–235.

- Jenkyns, C., Grficke, R., Hesselbo, P., & Holloway, R. (2001). Nitrogen isotope evidence for water mass denitrification during the early Toarcian (Jurassic) oceanic anoxic event Stephen Abstract . Bulk sedimentary nitrogen isotope data have been generated from Lower Jurassic excursion through the exaratum Subzone o, 16(6), 593–603.

- Jenkyns, H. C. (1985). The early Toarcian and Cenomanian-Turonian anoxic events in Europe: comparisons and contrasts. Geologische Rundschau, 74(3), 505–518. https://doi.org/10.1007/BF01821208

- Kafousia, N., Karakitsios, V., Jenkyns, H. C., & Mattioli, E. (2011). A global event with a regional character: the Early Toarcian Oceanic Anoxic Event in the Pindos Ocean (northern Peloponnese, Greece). Geological Magazine, 148(May), 619–631. https://doi.org/10.1017/S0016756811000082

- Korte, C., Hesselbo, S. P., Ullmann, C. V., Dietl, G., Ruhl, M., Schweigert, G., & Thibault, N. (2015). Jurassic climate mode governed by ocean gateway. Nature Communications, 6, 10015. https://doi.org/10.1038/ncomms10015

- Kranck, K., & Milligan, T. (1980). Macroflocs: Production of Marine Snow in the Laboratory. Marine Ecology, 3, 19–24. https://doi.org/10.3354/meps003019

- Lash, G. G. (2016). Hyperpycnal transport of carbonaceous sediment – Example from the Upper Devonian Rhinestreet Shale, western New York, U.S.A. Palaeogeography, Palaeoclimatology, Palaeoecology, 459, 29–43. https://doi.org/10.1016/j.palaeo.2016.06.035

- Lazar, O. R., Bohacs, K. M., Macquaker, J. H. S., Schieber, J., & Demko, T. M. (2015). Capturing Key Attributes of Fine-Grained Sedimentary Rocks In Outcrops, Cores, and Thin Sections: Nomenclature and Description Guidelines. Journal of Sedimentary Research, 85(3), 230–246. https://doi.org/10.2110/jsr.2015.11

- Loutit, T. S., Hardenbol, J., Vail, P. R., & Baum, G. R. (1988). Condensed sections: The key to age determination and correlatio of continental margin sequences. Sea-Level Changes (Vol. 42). https://doi.org/10.2110/pec.88.01.0183

- Macquaker, J. H. S., & Adams, a E. (2003). Maximizing Information from Fine-Grained Sedimentary Rocks: An Inclusive Nomenclature for Mudstones. Journal of Sedimentary Research, 73(5), 735–744. https://doi.org/10.1306/012203730735

- Macquaker, J. H. S., & Jones, C. R. (2002). A sequence-stratigraphic study of mudstone heterogeneity: A combined petrographic wireline log investigation of Upper Jurassic mudstones from the North Sea (U.K.). In Geological applications of well logs: AAPG Methods in Exploration No. 13, (pp. 123–141).

- Macquaker, J. H. S., Bentley, S. J., & Bohacs, K. M. (2010). Wave-enhanced sediment-gravity flows and mud dispersal across continental shelves: Reappraising sediment transport processes operating in ancient mudstone successions. Geology, 38(10), 947–950. https://doi.org/10.1130/G31093.1

- Macquaker, J. H. S., Taylor, K. G., & Gawthorpe, R. L. (2007). High-Resolution Facies Analyses of Mudstones: Implications for Paleoenvironmental and Sequence Stratigraphic Interpretations of Offshore Ancient Mud-Dominated Successions. Journal of Sedimentary Research, 77(4), 324–339. https://doi.org/10.2110/jsr.2007.029

- Mattioli, E., Pittet, B., Suan, G., & Mailliot, S. (2008). Calcareous nannoplankton changes across the early Toarcian oceanic anoxic event in the western Tethys. Paleoceanography, 23(3), 1–17. https://doi.org/10.1029/2007PA001435

- McArthur, J. M., Algeo, T. J., Van De Schootbrugge, B., Li, Q., & Howarth, R. J. (2008). Basinal restriction, black shales, Re-Os dating, and the Early Toarcian (Jurassic) oceanic anoxic event. Paleoceanography, 23(4), 1–22. https://doi.org/10.1029/2008PA001607

- Morten, S. D., & Twitchett, R. J. (2009). Fluctuations in the body size of marine invertebrates through the Pliensbachian-Toarcian extinction event. Palaeogeography, Palaeoclimatology, Palaeoecology, 284(1–2), 29–38. https://doi.org/10.1016/j.palaeo.2009.08.023

- Newton, R. J., Reeves, E. P., Kafousia, N., Wignall, P. B., Bottrell, S. H., & Sha, J. G. (2011). Low marine sulfate concentrations and the isolation of the European epicontinental sea during the Early Jurassic. Geology, 39(1), 7–10. https://doi.org/10.1130/G31326.1

- Nyhuis, C. J., Riley, D., & Kalasinska, A. (2016). Thin section petrography and chemostratigraphy: integrated evaluation of an upper Mississippian mudstone dominated succession from the southern Netherlands. Netherlands Journal of Geosciences/Geologie En Mijnbouw, 95(1), 3–22. https://doi.org/10.1017/njg.2015.25

- Percival, L. M. E., Cohen, A. S., Davies, M. K., Dickson, A. J., Hesselbo, S. P., Jenkyns, H. C., … Xu, W. (2016). Osmium isotope evidence for two pulses of increased

continental weathering linked to Early Jurassic volcanism and climate change. Geology, 44(9), 759–762. https://doi.org/10.1130/G37997.1

- Pilskaln, C. H., & Honjo, S. (1987). The Fecal Pellet fraction of biogeochemical particle fluxes to the deep sea. Global Biogeochemical Cycles, 1(1), 31–48. https://doi.org/10.1029/GB001i001p00031

- Plint A.G., In: James, N. P., Dalrymple, R. W., & Geological Association of Canada. (2010). Facies models 4. GEOtext. https://doi.org/9781897095508

- Plint, A. G., Macquaker, J. H. S., & Varban, B. L. (2012). Bedload Transport of Mud Across A Wide, Storm-Influenced Ramp: Cenomanian-Turonian Kaskapau Formation, Western Canada Foreland Basin. Journal of Sedimentary Research, 82(11), 801–822. https://doi.org/10.2110/jsr.2012.64

- Plint, A.G., Wave- And Storm-Dominated Shoreline And Shallow-Marine Systems, In: James, N.P., Dalrymple, R.W. (2010). Facies Models 4, Geological Association of Canada, 233-264.

- Potter, P. E., Maynard, J. B., & Depetris, P. J. (2005). Mud and mudstones: Introduction and overview. Mud and Mudstones: Introduction and Overview. https://doi.org/10.1007/b138571

- Prauss, M. L. (2007). Availability of Reduced Nitrogen Chemospecies in Photic-Zone Waters As the Ultimate Cause for Fossil Prasinophyte Prosperity, 22(5), 489–499. https://doi.org/10.2110/palo.2005.p05-095r

- Prauss, M., Ligouis, B., & Luterbacher, H. (1991). Organic matter and palynomorphs in the "Posidonienschiefer" (Toarcian, Lower Jurassic) of southern Germany. Geological Society, London, Special Publications, 58(1), 335–351. https://doi.org/10.1144/GSL.SP.1991.058.01.21

- Röhl, H. J., Schmid-Röhl, A., Oschmann, W., Frimmel, A., & Schwark, L. (2001). The Posidonia Shale (Lower Toarcian) of SW-Germany: An oxygen-depleted ecosystem controlled by sea level and palaeoclimate. Palaeogeography, Palaeoclimatology, Palaeoecology, 165(1–2), 27–52. https://doi.org/10.1016/S0031-0182(00)00152-8

- Röhl, H., & Schmid-Röhl, A. (2005). Lower Toarcian (Upper Liassic) Black Shales of the Central European Epicontinental Basin: a Sequence Stratigraphic Case Study From the Sw German Posidonia Shale. Special Publication-Sepm, (82), 165–189. https://doi.org/10.2110/pec.05.82.0165

- Schieber, J. (1990). Significance of styles of epicontinental shale sedimentation in the Belt basin, Mid-Proterozoic of Montana, U.S.A. Sedimentary Geology, 69(3–4), 297–312. https://doi.org/10.1016/0037-0738(90)90055-X

- Schieber, J. (2009). Discovery of agglutinated benthic foraminifera in Devonian black shales and their relevance for the redox state of ancient seas. Palaeogeography, Palaeoclimatology, Palaeoecology, 271(3–4), 292–300. https://doi.org/10.1016/j.palaeo.2008.10.027

- Schieber, J. (2011). Marcasite in Black Shales--a Mineral Proxy for Oxygenated Bottom Waters and Intermittent Oxidation of Carbonaceous Muds. Journal of Sedimentary Research, 81(7), 447–458. https://doi.org/10.2110/jsr.2011.41

- Schieber, J. (2016). Mud re-distribution in epicontinental basins - Exploring likely processes. Marine and Petroleum Geology, 71, 119–133. https://doi.org/10.1016/j.marpetgeo.2015.12.014

- Schouten, S., Van Kaam-Peters, H. M. E., Rijpstra, W. I. C., Schoell, M., & Sinninghe Damste, J. S. (2000). Effects of an oceanic anoxic event on the stable carbon isotopic composition of early Toarcian carbon. American Journal of Science, 300(1), 1–22. https://doi.org/10.2475/ajs.300.1.1

- Schwark, L., & Frimmel, A. (2004). Chemostratigraphy of the Posidonia Black Shale, SW-Germany II. Assessment of extent and persistence of photic-zone anoxia using aryl isoprenoid distributions. Chemical Geology, 206(3–4), 231–248. https://doi.org/10.1016/j.chemgeo.2003.12.008

- Sinninghe Damsté, J. S., & Köster, J. (1998). A euxinic southern North Atlantic Ocean during the Cenomanian/Turonian oceanic anoxic event. Earth and Planetary Science Letters, 158(3–4), 165–173. https://doi.org/10.1016/S0012-821X(98)00052-1

- Song, J., Littke, R., Weniger, P., Ostertag-Henning, C., & Nelskamp, S. (2015). Shale oil potential and thermal maturity of the Lower Toarcian Posidonia Shale in NW Europe. International Journal of Coal Geology, 150–151, 127–153. https://doi.org/10.1016/j.coal.2015.08.011

- Svensen, H., Planke, S., Chevallier, L., Malthe-Sørenssen, A., Corfu, F., & Jamtveit, B. (2007). Hydrothermalventing of greenhouse gases triggering Early Jurassic global warming. Earth and Planetary Science Letters, 256(3–4), 554–566. https://doi.org/10.1016/j.epsl.2007.02.013

- Suan, G., Nikitenko, B. L., Rogov, M. A., Baudin, F., Spangenberg, J. E., Knyazev, V. G., … Lécuyer, C. (2011). Polar record of Early Jurassic massive carbon injection. Earth and Planetary Science Letters, 312(1–2), 102–113. https://doi.org/10.1016/j.epsl.2011.09.050

- Suan, G., Pittet, B., Bour, I., Mattioli, E., Duarte, L. V., & Mailliot, S. (2008). Duration of the Early Toarcian carbon isotope excursion deduced from spectral analysis: Consequence for its possible causes. Earth and Planetary Science Letters, 267(3–4), 666–679. https://doi.org/10.1016/j.epsl.2007.12.017

- Suan, G., van de Schootbrugge, B., Adatte, T., Fiebig, J., & Oschmann, W. (2015). Calibrating the magnitude of the Toarcian carbon cycle perturbation. Paleoceanography. https://doi.org/10.1002/2014PA002758

- Trabucho-Alexandre, J., Dirkx, R., Veld, H., Klaver, G., & de Boer, P. L. (2012). Toarcian Black Shales In the Dutch Central Graben: Record of Energetic, Variable Depositional Conditions During An Oceanic Anoxic Event. Journal of Sedimentary Research, 82(2), 104–120. https://doi.org/10.2110/jsr.2012.5

- Turner, J. T. (2002). Zooplankton fecal pellets, mrine snow and sinking phytoplankton blooms. Aquatic Microbial Ecology, 27, 57–102. https://doi.org/Doi 10.3354/Ame027057

- Turner, J. T. (2015). Zooplankton fecal pellets, marine snow, phytodetritus and the ocean's biological pump. Progress in Oceanography, 130, 205–248. https://doi.org/10.1016/j.pocean.2014.08.005

- van de Schootbrugge, B., & Wignall, P. B. (2016). A tale of two extinctions: converging end-Permian and end-Triassic scenarios. Geological Magazine, 153(02), 332-354.

- Van de Schootbrugge, B., Bachan, A., Suan, G., Richoz, S., & Payne, J. L. (2013). Microbes, mud and methane: Cause and consequence of recurrent early Jurassic anoxia following the end-Triassic mass extinction. Palaeontology, 56(4), 685–709. https://doi.org/10.1111/pala.12034

- Van de Schootbrugge, B., McArthur, J. M., Bailey, T. R., Rosenthal, Y., Wright, J. D., & Miller, K. G. (2005). Toarcian oceanic anoxic event: An assessment of global causes using belemnite C isotope records. Paleoceanography, 20(3), 1–10. https://doi.org/10.1029/2004PA001102

- Vigran, J. O., Mark, A., Forsberg, A. W., Weiss, H. M., & Weitschat, W. (2008). Tasmanites algae - Contributors to the Middle Triassic hydrocarbon source rocks of Svalbard and the Barents Shelf. Polar Research, 27(3), 360–371. https://doi.org/10.1111/j.1751-8369.2008.00084.x

- Visscher, H., Looy, C. V., Collinson, M. E., Brinkhuis, H., Van Konijnenburg-Van Cittert, J. H., Kürschner, W. M., & Sephton, M. A. (2004). Environmental mutagenesis during the end-Permian ecological crisis. Proceedings of the National Academy of Sciences of the United States of America, 101(35), 12952-12956.

- Wignall, P. B. (1991). Model for transgressive black shales? Geology. https://doi.org/10.1130/0091-7613(1991)019<0167:MFTBS>2.3.CO;2

- Wignall, P. B., & Bond, D. P. G. (2008). The end-Triassic and Early Jurassic mass extinction records in the British Isles. Proceedings of the Geologists' Association, 119(1), 73–84. https://doi.org/10.1016/S0016-7878(08)80259-3

- Wignall, P. B., Newton, R. J., & Little, C. T. S. (2005). The timing of paleoenvironmental changes and cause-and-effect relationships during the early Jurassic mass extinction in Europe. American Journal of Science, 305, 1014–1032.

- Wild, C., Roy, H., & Huettel, M. (2005). Role of pelletization in mineralization of fine-grained coastal sediments. Marine Ecology Progress Series, 291(Marinelli 1992), 23–33. https://doi.org/10.3354/meps291023

- Ziegler, P.A., 1982, Geological Atlas of Central and Western Europe: Amsterdam, Shell International Petroleum Maatschappij B.V., 130 p.

APPENDIX 1

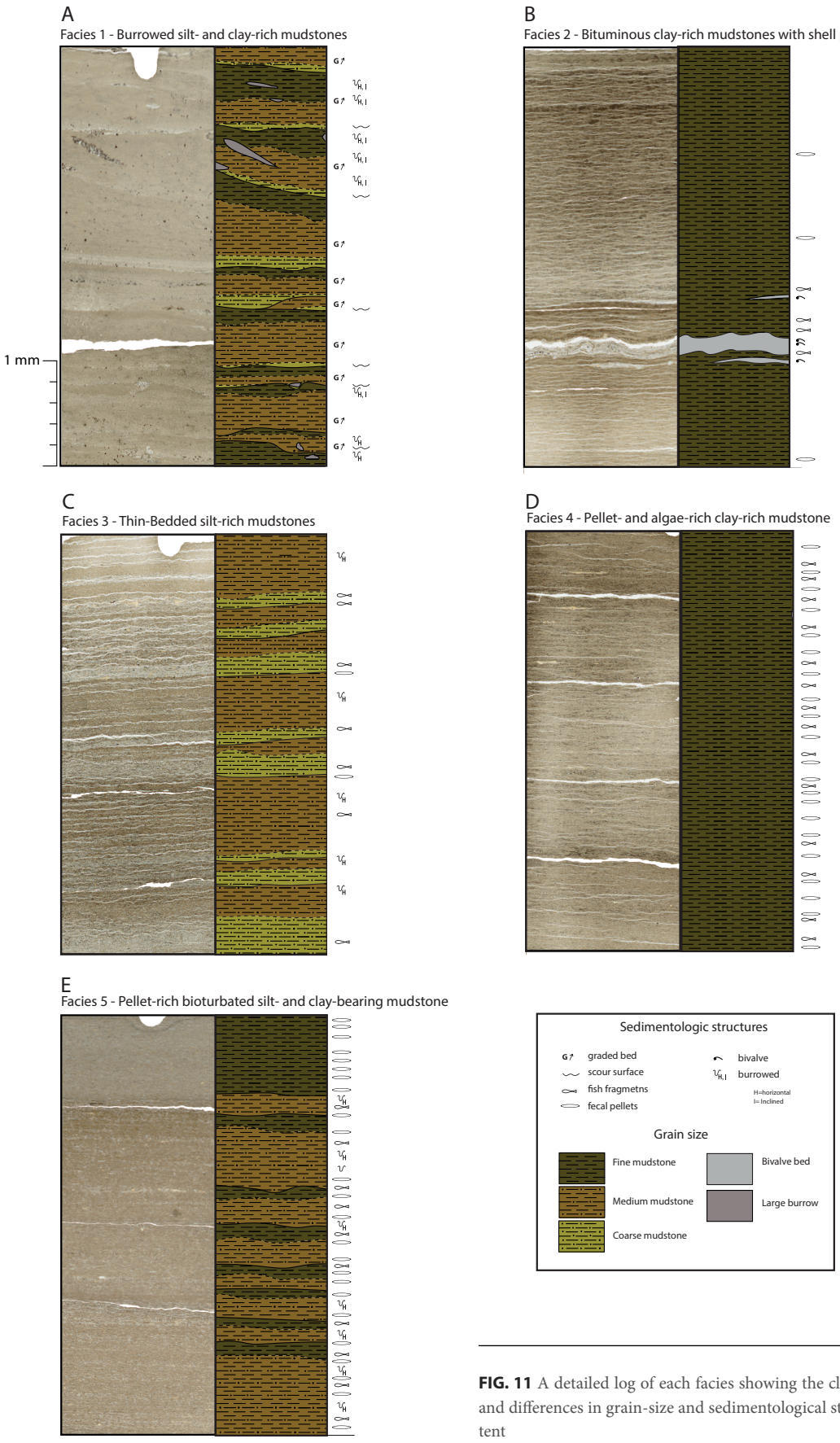

FIG. 11 A detailed log of each facies showing the clear characteristics and differences in grain-size and sedimentological structures and content

APPENDIX 2

Depth (mbsf)	Zone	Microfacies	Amorphic	Pollen	Spores	Dinoflagellates	Acritarcs	Prasinophytes
			%	%	%	%	%	%
30,00	*H. Bifrons*	5	80	<5	<5	<1	<1	5
30,22	*H. Bifrons*	5	95	<1	<1	<1	<1	5
30,60	*H. Bifrons*	5	90	<1	<1	<1	<1	5
31,30	*H. Bifrons*	5	95	<1	<1	<1	<1	5
31,60	*H. Bifrons*	5	85	<1	<1	<1	<1	7,5
32,00	*H. Falciferum*	4	75	5	<5	<1	<1	5
32,50	*H. Falciferum*	4	90	<1	<1	<1	<1	7,5
33,20	*H. Falciferum*	4	90	<5	<1	<1	<1	7,5
33,80	*H. Falciferum*	4	85	<1	<1	<1	<1	7,5
34,00	*H. Falciferum*	4	75	10	<5	<1	<1	10
34,40	*H. Falciferum*	4	85	<1	<1	<1	<1	15
34,80	*H. Falciferum*	4	85	<1	<1	<1	<1	15
35,20	*H. Falciferum*	4	85	<1	<1	<1	<1	15
36,00	*H. Falciferum*	4	85	<1	<1	<1	<1	10
36,50	*H. Falciferum*	4	85	<1	<1	<1	<1	10
36,90	*H. Falciferum*	4	85	<1	<1	<1	<1	10
37,40	*H. Falciferum*	4	85	<1	<1	<1	<1	10
37,70	*H. Falciferum*	4	85	<1	<1	<1	<1	10
38,00	*H. Falciferum*	4	90	<1	<1	<1	<1	10
38,30	*H. Falciferum*	4	90	<1	<1	<1	<1	10
39,40	*H. Falciferum*	3	90	<1	<1	<1	<1	10
39,90	*H. Falciferum*	3	90	<5	<5	<1	<1	7,5
40,00	*H. Falciferum*	3	90	<5	<5	<1	<1	7,5
40,40	*H. Falciferum*	3	90	<1	<1	<1	<1	7,5
41,00	*H. Falciferum*	3	90	<5	<1	<1	<1	10
42,00	*H. Falciferum*	2	90	<1	<1	<1	<1	10
42,50	*H. Falciferum*	2	90	<1	<1	<5	<5	10
42,90	*H. Falciferum*	2	85	<1	<1	<5	<5	10
43,10	*D. Tenuicostatum*	1	<1	60	10	5	5	<1
44,00	*D. Tenuicostatum*	1	<1	60	10	5	5	<1

TABLE 2. Summary of the studied thin sections of the Schandelah Core. From left to right: Depth (mbs), zone, sedimentological description, facies, grain-size, observed structures and carbon isotope values